Stochastic ground-motion prediction equations for southeastern Australian earthquakes using updated source and attenuation parameters

T.I. Allen

Stochastic ground-motion prediction equations for southeastern Australian earthquakes using updated source and attenuation parameters

by

T.I. Allen

Australian Government

Geoscience Australia

Contents

List of Figures

List of Tables

Executive Summary

Stochastic finite-fault ground-motion prediction equations (GMPEs) are developed for the stable continental region of southeastern Australia (SEA). The models are based on reinterpreted source and attenuation parameters for small-to-moderate magnitude local earthquakes and a dataset augmented with ground-motion records from recent well-recorded moderate-magnitude earthquakes relative to those used in prior studies (Allen *et al.*, 2007). The models are applicable for median horizontal-component ground-motions for earthquakes of moment magnitude 4.0 <= M_W <= 7.5 and at rupture distances less than 400 km.

Careful analysis of well-constrained Brune stress drops indicates an apparent dependence on hypocentral depth. It is speculated that this is the effect of an increasing crustal stress profile with depth. However, rather than a continuous increase, the change in stress drop appears to indicate a discrete step near 10 km depth. Average Brune stress drops for SEA earthquakes shallower and deeper than 10 km are estimated to be 23 MPa and 50 MPa, respectively. These stress parameters are subsequently input into the stochastic ground-motion simulations for the development of two discrete GMPEs for shallow and deep events.

The GMPEs estimate response spectral accelerations that are similar to the Atkinson and Boore (2006) GMPE for eastern North America (ENA) at short rupture distances (less than approximately 100 km). However, owing to higher attenuation observed in the SEA crust (Allen and Atkinson, 2007), the SEA GMPEs estimate lower median ground-motions than ENA models at larger distances. These differences become most obvious at distances greater than 200 km.

A correlation between measured near-surface shear-wave velocity, defined as the time-averaged shear-wave velocity in the top 30 m of the site profile (V_{S30}), and the site-dependent diminution term (κ_0) was developed from the limited data available to determine the average site condition to which the GMPEs are applicable. Assuming the correlation holds, a V_{S30} of approximately 820 m/s is obtained assuming an average path-independent diminution term κ_0 of 0.006 s from SEA seismic stations. Consequently, the GMPE presented herein can be assumed to be appropriate for rock sites of approximately B/C site class in the modified National Earthquake Hazards Reduction Program (Wills *et al.*, 2000; Building Seismic Safety Council, 2003) site classification scheme.

The response spectral models are compared against moderate-magnitude (4.0 <= M_W <= 5.3) earthquakes from eastern Australia. Overall the SEA GMPEs show low median residuals across the full range of spectral period and distances considered. In contrast, ENA models tend to overestimate response spectra at larger distances. Because of these differences, the present analysis justifies the need to develop Australian-specific GMPEs where ground-motion hazard from a distant seismic source may become important.

Introduction

Although the likelihood of a large earthquake occurring in a major urban centre is much lower in Australia than in more seismically active regions of the world (e.g., western North America, Japan and New Zealand), intraplate earthquakes have the potential to produce significant damage to property and critical infrastructure. This was poignantly demonstrated by the devastating 1989 Newcastle, New South Wales, earthquake (local magnitude M_L 5.6 [M_W 5.4], McCue *et al.*, 1990; Dhu and Jones, 2002). Despite being a moderate-sized earthquake by global standards, the event claimed 13 lives and caused extensive damage to many buildings; particularly, poor quality un-reinforced masonry structures (McCue *et al.*, 1990; Geoscience Australia, 2004). The 1989 Newcastle earthquake resulted in approximately AU\$3.2 billion in insured losses (2011 dollars) and remains one of Australia's most costly natural disasters (Insurance Council of Australia, 2012).

To support the update of future earthquake loading standards in Australia (Standards Australia, 2007), Geoscience Australia is developing a revised national earthquake hazard map through a rigorous probabilistic seismic hazard analysis (Burbidge *et al.*, 2010; Burbidge, 2012). Ground-motion prediction equations (GMPEs) are a critical component in any PSHA (e.g., Petersen *et al.*, 2008; Burbidge and Leonard, 2011) and underpin earthquake loading codes used in the design of engineered structures (Standards Australia, 2007). In designing a project to update Australia's National Earthquake Hazard Map, it was identified that there was a requirement to use of Australian-specific GMPEs where possible (Burbidge *et al.*, 2010). Allen (2010) summarises previous studies undertaken to evaluate ground-motion attenuation characteristics across the Australian stable continental region; from attenuation based on mean radii from isoseismal maps (e.g., Gaull *et al.*, 1990) through to modern GMPEs developed using sophisticated numerical simulation techniques (e.g., Lam and Wilson, 2008; Liang *et al.*, 2008; Somerville *et al.*, 2009). A subsequent review of Australian-specific GMPEs and those developed for other regions against recorded ground-motions by Allen *et al.* (2011) indicated that two of the models (Atkinson and Boore, 2006; Chiou and Youngs, 2008) appeared to approximate Australian ground-motions at periods appropriate for the national hazard model at short source-receiver distances. For the national hazard model, we are most interested in short period ground motions (i.e. peak ground acceleration), and the conclusions inferred by Allen *et al.* (2011) reflect this requirement. However, the long-distance characteristics of the aforementioned models are not appropriate for the attenuation of ground-motion observed in southeastern Australia (Allen *et al.*, 2011). To capture the epistemic uncertainty, due to lack of knowledge, it is has become standard practice to use multiple GMPEs in a weighted logic tree analysis for probabilistic seismic hazard analysis (PSHA) (e.g., Bommer *et al.*, 2005). Consequently, a need was seen to incorporate additional GMPEs that were more representative of ground-motions observed in Australia into the national hazard model.

There is currently a major effort to develop a new suite of GMPEs for the Central and Eastern United States (CEUS) – a region often thought to be tectonically analogous to Australia – through the Next Generation Attenuation (NGA)-East Project (Goulet *et al.*, 2011). While Australian ground-motion data have been contributed to this effort and the deliverables from this Project will be highly relevant to seismic hazard applications throughout Australia, the outcomes of the NGA-East Project were not available for the revision of the 2012 Australian National Earthquake Hazard Map (ANEHM).

This manuscript outlines the development of a stochastic GMPE developed from source and attenuation parameters derived from a suite of ground-motion data recorded in southeastern Australia (SEA). The source and attenuation parameters provided in Allen *et al.* (2007) are first reviewed and modified in light of additional data and more rigorous statistical analysis. This includes the revision of geometrical attenuation and anelastic attenuation models, which subsequently allow the update of earthquake source parameters: moment magnitude and stress drop. The dependence of stress drop on hypocentral depth is examined, and options are provided for variable Brune stress drops in the predictive GMPE. The near-surface, path-independent diminution parameter immediately beneath the station, κ_0, (Anderson and Hough, 1984; Campbell, 2009; Van Houtte *et al.*, 2011) is also examined for average station conditions in SEA, in addition to the parameter's correspondence with a limited dataset of time-averaged shear-wave velocity measurements in the upper 30 m (V_{S30}) at seismic recording stations across Australia.

Finally, the updated source and attenuation parameters are used as inputs to the stochastic finite-fault software package, EXSIM (Motazedian and Atkinson, 2005; Atkinson and Boore, 2006). Five-percent damped response spectral accelerations are simulated for earthquakes of moment magnitude M_W 4.0 to 7.5. These stochastic data are then regressed to obtain model coefficients and the resulting model is evaluated against recorded response spectral data for moderate-magnitude earthquakes recorded in southeastern Australia. The products presented herein provide an improved prediction of earthquake ground-shaking potential in Australia for the Australian National Earthquake Hazard Map (ANEHM) and future PSHA studies. Furthermore, the models have the potential to provide critical decision support information for planners and emergency managers involved in disaster mitigation and response.

Stochastic Method

The stochastic method is particularly useful for simulating earthquake ground-motions in regions of the world where recordings from large damaging earthquakes are simply not available (Boore, 1983; 2003) and has been used in several commonly-used GMPEs for global stable continental regions (Boore and Atkinson, 1987; Toro *et al.*, 1997; Bay *et al.*, 2005; Atkinson and Boore, 2006; Rietbrock *et al.*, in press). The stochastic finite-fault simulation software EXSIM (Motazedian and Atkinson, 2005) is used to simulate the magnitude dependence on ground-shaking for larger earthquakes in southeastern Australia. This version of the software has been used successfully to develop ground-motion attenuation models for ENA (Atkinson and Boore, 2006). It has since been recognised by Atkinson *et al.* (2009), however, that finite-fault ground-motion simulations for small earthquakes (approximately M_W 5.0) using this version of EXSIM do not compare well with point source simulations (e.g., Boore, 2003) at large distances ($R \geq 100$ km), where it should be expected that the two simulation techniques would agree. In a companion article, Boore (2009) finds that high-frequency Fourier amplitude spectra from the extended fault method (EXSIM) are lower than point source simulations from the program SMSIM (Boore, 2003). It was observed by Boore (2009) that the differences between EXSIM and SMSIM were minimised if fewer sub-faults were used and sub-fault "pulsing" was considered. The pulsing term is incorporated to consider that only part of the fault may be actively rupturing at any one time. In such a model, the areas that are actively pulsing contribute to the ground-motion radiation, but the other areas on the fault are passive (Motazedian and Atkinson, 2005). To address this discrepancy, Boore (2009) recommended several enhancements to the Motazedian and Atkinson (2005) implementation of EXSIM.

The Motazedian and Atkinson (2005) implementation of EXSIM as used in Atkinson and Boore (2006) was extensively modified for the purpose of randomising the input stochastic parameters for GMPE development. Unfortunately, this functionality was not carried through to the most recent update of EXSIM (David Boore, pers. comm., 2012). Due to time restrictions in developing an effective GMPE for eastern Australia that could be used for the ANEHM, I use the Motazedian and Atkinson (2005) implementation of EXSIM and attempt to minimise the aforementioned discrepancies between finite-fault and point-source simulations by using fewer sub-faults and by applying a 25% pulsing source.

In practice, the observed earthquake displacement spectrum of the shear wave on rock, $A(M_0, R, f)$, can be generalized as the convolution of several factors; the earthquake point source spectrum, the propagation path that incorporates both geometrical and anelastic attenuation, and path-independent diminution such that:

$$A(M_0, R, f) = CM_0 \left[1 + (f/f_0)^2 \right]^{-1} \exp(-\pi f R / Q\beta) \exp(-\pi f \kappa) R^{-b} \tag{1}$$

where ground-motion is dependent on the seismic moment M_0, the frequency of motion f and the hypocentral distance R. The constant C is given by $\Re_{\theta\phi} FV/(4\pi\rho\beta^3)$, where $\Re_{\theta\phi} = 0.55$ is the average radiation pattern (Boore and Boatwright, 1984), $F = 2$ is the free-surface amplification, $V = 0.71$ represents the partition to two horizontal components, ρ is the density in kg/m^3 and β is the shear-wave velocity in m/s (Boore, 2003). The corner frequency of the Fourier displacement spectrum is given by f_0. The seismic quality factor Q represents a measure of the anelastic attenuation through the propagation path, κ_0 is the near-surface diminution term which affects the high-frequency component of the Fourier spectrum and b is the geometrical attenuation coefficient, which approximates the spreading of shear-waves in a whole space. In theory, b is equal to 1.0 for body-wave spreading (Aki and Richards, 2002), but may vary owing to deviations in crustal attenuation properties and the arrival of other phases within the shear-wave window; for example, postcritical reflections from the Moho or other mid-crustal discontinuities (Ou and Herrmann, 1990; Atkinson, 2004; Allen *et al.*, 2007). Table 1 provides a listing of the key aforementioned parameters as well as those introduced later.

Table 1: A description of selected key parameters introduced in this manuscript

PARAMETER	UNITS	DESCRIPTION
M_0	N-m	Seismic moment
R	km	Hypocentral distance
R_{rup}	km	Closest distance to rupture
f	Hz	Number of cycles per second
f_0	Hz	The corner frequency, or the frequency at which the high-frequency displacement spectrum begins to decay as a function of ω^2 [$= (2\pi f)^2$]
$\Delta\sigma$	MPa	The Brune (1970,1971) stress drop
$Q(f)$	-	The frequency-dependent seismic *quality factor* or the *anelastic attenuation factor* which accounts for the attenuation of seismic signal through internal absorption and scattering
κ_0	s	Path-independent site attenuation parameter (kappa)
V_{S30}	m/s	Average shear-wave velocity in the upper 30 m of the crust
b'	-	Initial starting value of near-source ($R < 100$ km) geometrical attenuation used in the data normalisation process to solve for the final geometrical attenuation factors
b_1	-	Geometrical attenuation coefficient for $R \leq 90$ km
b_2	-	Geometrical attenuation coefficient for $90 \leq R \leq 150$ km
b_3	-	Geometrical attenuation coefficient for $R > 150$ km
$A_{ij}(f)$	m-s	Frequency dependent Fourier displacement spectra at a site R kilometres from the seismic source for earthquake i at site j
$A_{0,i}(f)$	m-s	Estimated Fourier displacement source spectrum for event i
$A_{n,ij}(f)$	-	Normalised Fourier displacement amplitude for an earthquake i at the jth site
$A_{g,ij}(f)$	-	Normalised Fourier displacement amplitudes corrected for geometrical attenuation
$A_{q,ij}(f)$	-	Normalised Fourier displacement amplitudes corrected for both geometrical attenuation and anelastic attenuation
$a_{\kappa,ij}(f)$	-	Fourier acceleration amplitudes, corrected for attenuation and anelastic attenuation and normalised at 2 Hz
$Y(T)$	cm/s^2	Five percent damped pseudo response spectral acceleration (RSA) for median horizontal component ground motions.

The use of stochastic finite-fault methods are important for improving our estimates of strong ground shaking for larger earthquakes where point source models become inappropriate, particularly at short source-receiver distances (Atkinson and Boore, 2006). The method employed by EXSIM is to divide the simulated rupture plane into a number of sub-faults, each of which is modelled as a small point source (e.g., Hartzell, 1978). The total contribution from each sub-fault at an observation point is then summed to provide an estimate of the ground-shaking from the full rupture assuming appropriate time delays. More detailed discussion of this technique is described in Motazedian and Atkinson (2005).

In the present study, the EXSIM FORTRAN code enabled to randomise source and attenuation properties for GMPE development have been modified to accommodate the alternative anelastic attenuation model described below, and also to incorporate the Leonard (2010) fault scaling relations appropriate for stable continental regions rather than the Wells and Coppersmith (1994) relations. The empirical analysis of source and path parameters uses hypocentral distance R. For the small-magnitude earthquakes investigated, it is assumed that hypocentral distance and closest distance to

rupture are equivalent. Consequently, the attenuation parameters derived from the point source hypocentral distance measurements are assumed to be applicable for forward modelling of larger-magnitude earthquake ground-motions.

Dataset and Ground-Motion Data Preparation

In updating earthquake source and attenuation parameters, the dataset used by Allen *et al.* (2007) is augmented with data recorded from recent earthquakes. The inclusion of data is limited by the magnitude-distance criterion employed by Atkinson (2004) to eliminate low-amplitude quantization noise problems. Figure 1 indicates the magnitude-distance distribution of the datasets. The magnitude of all events is represented by moment magnitude M_W and is calculated using the updated attenuation parameters determined from the present analysis. The spatial distribution of the dataset is indicated in Figure 2. The dataset comprises some 1,079 strong- and weak-motion records from 75 earthquakes (Table 2). These events range in magnitude from moment magnitude $2.8 \leq M_W \leq 5.4$ recorded between 1989 and 2011.
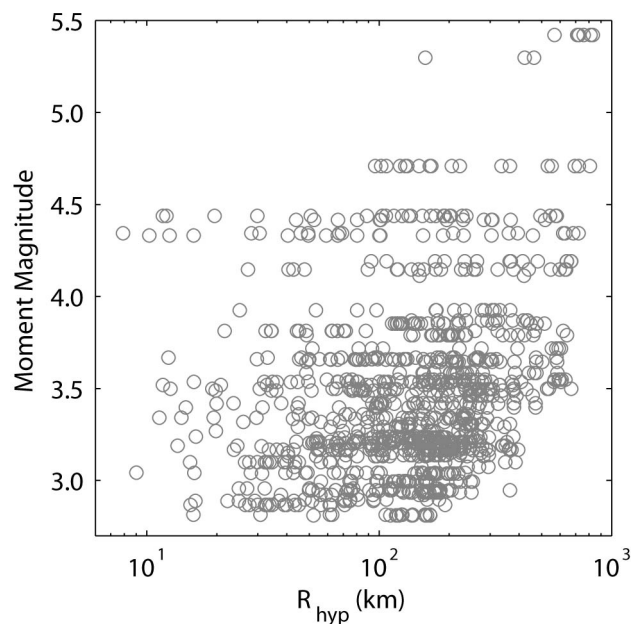
Figure 1: *Magnitude-distance distribution of the southeastern Australian (SEA) dataset used to derive the stochastic suite of parameters. Moment magnitudes, M_W, are calculated using the attenuation parameters derived in the present study.*

Note that many of the data employed from SEA were recorded on short-period weak-motion instruments with natural frequencies at 1.0 or 2.0 Hz (Allen *et al.*, 2007). While every effort was made to correct for instrument response, the limited bandwidth of many of the instruments makes the data potentially less reliable at frequencies lower than the instrumental natural frequency.

Windowed shear-wave displacement spectra were calculated and smoothed using the spline interpolation algorithm to minimize the effect of extreme Fourier spectral values. The shear window length varied for each record, with each window chosen to include the strongest shaking. A series of 22 discrete amplitudes were extracted from each record, logarithmically distributed from 0.2 to 24 Hz. An average pre-event noise spectrum was also calculated for each station. For each frequency of ground-shaking, data less than twice the average noise spectrum are removed from the analysis (e.g., Atkinson and Mereu, 1992). Because the majority of the weak-motion data used in the empirical analysis were recorded at 100 samples per second, Fourier spectral frequencies at frequencies greater than 25 Hz were not considered owing to Nyquist frequency and aliasing effects.

Table 2: *List of earthquakes used in the present analysis. Moment magnitude M_W and Brune stress drop $\Delta\sigma$ were calculated using the attenuation parameters derived in the present study and fitting corrected Fourier displacement source spectra (see Fig. 11). While stress drops were estimated for all events, only the most well-constrained values are included herein and used for further analysis. The distance range indicates the minimum and maximum hypocentral distance of stations used. Those events with an asterisk (*) have three or more stations at hypocentral distances less than 100 km, and these events were used to determine the path parameters.*

ORIGIN	LOCATION	LONGITUDE	LATITUDE	DEPTH (km)	M_W	STRESS DROP (MPa)	NO. RECS	DISTANCE RANGE (km)
1989-12-27 23:24	Newcastle, NSW	151.61	-32.95	10.5	5.4		7	568.2-829.2
1993-07-24 13:33	Churchill, VIC	146.49	-38.35	15.0	3.2		5	31.2-277.0
1993-09-25 02:40	Traralgon South, VIC	146.53	-38.31	10.2	3.3		7	26.0-214.9*
1994-02-01 05:53	Boolarra South, VIC	146.35	-38.54	17.1	3.7		12	51.5-605.3
1994-05-21 08:59	Ettamogah, NSW	146.96	-36.03	3.0	3.2		8	71.9-364.3
1994-08-06 11:03	Ellalong, NSW	151.29	-32.92	0.6	4.7	20.7	19	96.1-805.6
1995-01-03 13:51	Bowral, NSW	150.48	-34.53	7.0	2.9		10	16.2-94.4*
1995-01-11 07:11	Warragul, VIC	145.99	-38.17	8.7	3.1		5	40.5-274.4
1995-02-01 10:21	Boolarra South, VIC	146.26	-38.46	10.1	3.1		5	43.2-294.6
1995-03-26 06:53	Dora Dora, NSW	147.23	-35.96	3.7	3.2		11	13.6-350.2*
1995-05-03 04:24	Newnes, NSW	150.25	-33.19	10.7	3.2		18	53.7-245.5
1995-05-03 17:48	Boolarra South, VIC	146.28	-38.47	15.0	3.4		8	45.0-240.4*
1995-05-20 11:29	Jenolan Caves, NSW	150.08	-33.87	13.8	3.5		16	19.8-379.3*
1995-07-21 14:26	Adaminaby, NSW	148.86	-36.03	4.8	3.3		17	121.6-364.8
1995-07-29 13:43	Frogmore, NSW	148.74	-34.28	2.8	2.9		11	75.2-196.1
1995-07-30 04:41	Benambra, VIC	147.66	-36.76	11.3	3.5	63	15	11.7-377.0*
1995-08-17 01:41	Boorowa, NSW	148.74	-34.31	3.6	2.9		16	71.9-249.3
1995-08-19 09:01	Boorowa, NSW	148.74	-34.31	1.3	3.1		20	71.8-296.2
1995-09-12 10:23	Boorowa, NSW	148.72	-34.31	1.1	3.2		20	71.6-295.5
1995-10-14 04:11	Frogmore, NSW	148.76	-34.32	3.0	3.2		21	71.0-295.9
1995-11-18 09:32	Tooborac, VIC	144.76	-37.11	13.5	3.5		21	59.5-633.1

ORIGIN	LOCATION	LONGITUDE	LATITUDE	DEPTH (km)	M_W	STRESS DROP (MPa)	NO. RECS	DISTANCE RANGE (km)
1996-01-16 10:30	Mt Martha, VIC	145.07	-38.28	10.7	3.0		7	74.5-130.6
1996-02-18 19:34	Eucumbene, NSW	148.67	-36.15	12.8	3.5		18	81.2-430.0
1996-05-10 05:48	Toorongo, VIC	146.15	-37.73	10.6	3.0		10	24.9-177.8*
1996-08-13 12:33	Dalton, NSW	149.21	-34.75	1.0	3.0		21	56.1-252.7
1996-09-25 04:53	Thomson Reservoir, VIC	146.43	-37.86	10.8	3.3		16	11.3-237.8*
1996-09-25 07:49	Thomson Reservoir, VIC	146.42	-37.86	11.4	4.4	106.9	26	11.7-580.9*
1996-10-01 21:42	Katoomba, NSW	150.39	-33.83	8.7	3.2		21	23.7-396.6*
1996-12-10 12:54	Thirlmere, NSW	150.50	-34.15	12.3	3.1		22	15.3-385.7*
1996-12-10 12:58	Thirlmere, NSW	150.50	-34.15	12.4	2.9		17	15.4-192.1*
1996-12-24 22:28	Cape Paterson, VIC	145.53	-38.70	17.2	3.3		12	44.7-345.5
1997-05-04 22:33	Warragul, VIC	145.96	-38.14	14.0	3.2		11	44.0-223.8*
1997-06-27 03:20	Tatong, VIC	146.09	-36.78	8.6	3.9	17.2	23	113.5-514.5
1997-08-23 00:13	Cootamundra, NSW	148.20	-34.63	3.6	3.2		17	54.3-246.1
1998-02-14 18:23	Brindabella, NSW	148.70	-35.38	8.5	3.8	123.7	23	48.7-642.4
1998-03-09 12:41	Merriwa, NSW	150.06	-32.17	3.7	3.3		10	132.5-290.8
1998-04-04 09:55	Fish Creek, VIC	146.12	-38.71	16.2	3.4		11	20.0-325.2
1998-07-17 01:22	Corryong, NSW	148.01	-36.44	20.3	3.9		14	25.1-365.6*
1998-11-07 22:42	Wee Jasper, NSW	148.89	-35.14	6.7	3.0		17	31.3-219.0
1998-12-31 06:11	Michelago, NSW	149.15	-35.78	4.4	3.2		17	103.0-353.9
1999-01-13 09:40	Yallourn North, VIC	146.32	-38.10	12.3	3.5	68.7	18	15.9-605.7*
1999-03-14 00:13	West Wyalong, NSW	147.07	-34.01	12.2	3.9		12	137.5-434.5
1999-03-17 01:58	Appin, NSW	150.75	-34.25	5.3	4.3	4.6	14	7.9-720.3*
1999-04-16 10:51	Lake Mountain, VIC	145.98	-37.41	3.6	3.2		17	49.9-203.2*
1999-04-16 11:08	Lake Mountain, VIC	145.97	-37.42	3.7	2.9		17	49.8-364.7*

ORIGIN	LOCATION	LONGITUDE	LATITUDE	DEPTH (km)	M_W	STRESS DROP (MPa)	NO. RECS	DISTANCE RANGE (km)
1999-07-13 01:42	Frogmore, NSW	148.98	-34.29	3.7	3.2		18	79.7-268.7
1999-08-19 17:10	Epping, VIC	144.99	-37.50	3.8	2.8		11	15.8-165.4*
1999-09-27 09:29	Dalton, NSW	149.16	-34.75	3.6	2.8		11	52.1-165.8
2000-03-16 13:26	Gaffneys Creek	146.10	-37.50	8.4	3.5		15	36.2-205.2*
2000-06-11 18:40	Boolarra South, VIC	146.30	-38.43	16.6	2.9		8	47.7-180.4*
2000-06-22 18:13	Graytown, VIC	144.86	-36.82	5.7	3.3		12	19.8-237.6*
2000-07-24 07:47	Dandenong, VIC	145.27	-37.96	19.5	3.1		11	40.6-280.7*
2000-08-03 11:29	Fish Creek, VIC	145.99	-38.75	16.2	3.2		13	16.2-377.5*
2000-08-29 10:20	Boolarra South, VIC	146.24	-38.39	14.6	3.0		13	16.0-234.1*
2000-08-29 12:05	Boolarra South, VIC	146.25	-38.40	15.1	4.1	95.7	24	27.2-636.4*
2001-01-05 16:04	Mt Worth, VIC	146.01	-38.26	8.0	2.9		8	37.7-155.8*
2001-08-21 23:13	Tooradin, VIC	145.45	-38.18	5.0	3.7		16	49.6-304.9*
2001-10-13 04:42	Benambra, VIC	147.69	-36.80	11.6	3.4		18	23.6-470.9*
2001-10-27 07:58	Swan Hill, VIC	143.39	-35.50	9.0	4.2	47.6	15	92.4-670.2
2001-11-23 03:33	Grenfell, NSW	148.39	-33.87	4.0	3.6	15	20	48.5-584.0
2002-02-14 13:27	Lake Avon, NSW	150.74	-34.52	5.0	3.5		16	12.6-669.5*
2002-08-22 21:23	Grenfell, NSW	148.35	-33.87	3.0	3.6	24.1	19	48.5-582.7
2002-09-24 07:42	Fish Creek, VIC	146.08	-38.67	3.4	3.7	29.7	19	12.4-578.6*
2002-09-24 13:39	Fish Creek, VIC	146.10	-38.66	5.0	3.4		19	14.7-470.6*
2003-12-11 10:19	Bowral, NSW	150.44	-34.49	13.3	3.8	43.1	19	21.6-618.1*
2004-02-28 11:32	Junee, NSW	147.68	-35.00	12.3	3.5		18	89.0-457.4
2007-03-08 02:34	Gilderoy, VIC	145.74	-37.90	9.7	3.7		18	29.7-319.3*
2009-01-12 08:48	Korumburra, VIC	145.87	-38.42	10.0	3.5	15.2	9	49.6-303.9*
2009-03-06 09:55	Korumburra, VIC	145.86	-38.41	17.3	4.4	60.8	14	43.9-517.5*

ORIGIN	LOCATION	LONGITUDE	LATITUDE	DEPTH (km)	M_W	STRESS DROP (MPa)	NO. RECS	DISTANCE RANGE (km)
2009-03-09 06:39	Korumburra, VIC	145.86	-38.40	7.6	3.3	14.0	7	42.5-228.2*
2009-03-18 05:28	Korumburra, VIC	145.87	-38.42	10.0	4.3	77.2	18	10.3-458.4*
2009-03-18 08:57	Korumburra, VIC	145.87	-38.40	8.8	3.0		7	9.0-153.0*
2011-04-16 05:31	Bowen, QLD	147.76	-20.09	7.0	5.3	29.3	3	157.7-463.0
2011-04-16 07:06	Bowen, QLD	147.68	-20.17	7.0	4.1		2	149.1-419.5
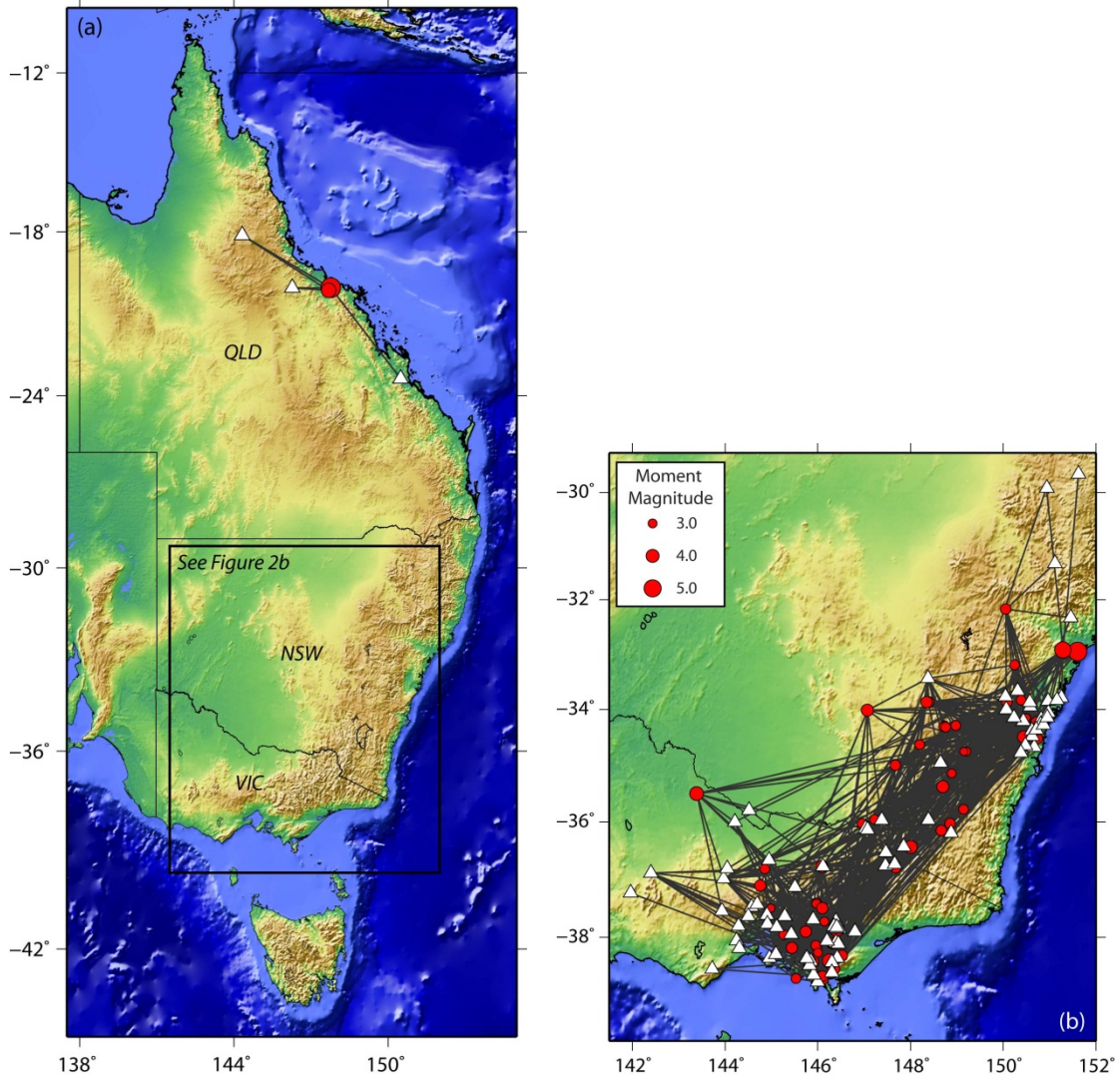
Figure 2: *Spatial distribution of SEA earthquakes in the states of New South Wales (NSW), Victoria (VIC) and Queensland (QLD). (a) Two moderate-sized earthquakes from Queensland (QLD) are also included in the primary dataset (b). Solid black circles and white triangles indicate earthquake epicenters and locations of recording stations, respectively. Grey lines indicate ray paths uses in the present analysis.*

Since there are a limited number of data with which to perform regressions in any one-magnitude range, Fourier amplitude spectra were normalised to obtain attenuation coefficients (geometrical attenuation and anelastic attenuation) for the southeastern Australian dataset. This process, which is described in more detail below, was performed so that all data could be considered in the single regression. An initial assumption is made such that low-frequency earthquake source spectra (i.e., R = 1.0 km) can be approximated by multiplying observed spectra by a factor of $R^{-b'}$ for all ground-motions recorded at hypocentral distances $R < 100$ km. The coefficient b' is an initial assumption of the near-source geometrical attenuation coefficient. This assumption should not precondition the final geometrical attenuation coefficients since this process is performed to estimate an approximate within-event source spectrum from which to normalise the data for a single earthquake i.

Only earthquakes recorded on three or more stations at distances $R \leq 100$ km – with at least one station at a distance $R \leq 50$ km – are used to estimate the initial geometrical attenuation coefficient b'. Fourier spectral displacements log $A_{ik}(f)$ at 2 Hz for each earthquake i are regressed against log R using linear least squares, where k represent the sites that satisfy the hypocentral distance criterion

above. The within-event geometrical attenuation was then aggregated and the median value was used as the initial assumption for the near source geometrical attenuation exponent, *b'*. Figure 3 plots the histogram of within-event geometrical attenuation at 2 Hz for all earthquakes with three stations less than 100 km from the earthquake source. Based on this analysis, an initial value of *b'* = -1.29 was used for the optimization of the geometrical attenuation parameters for the full wave path. The frequency of 2 Hz was chosen to model the geometrical attenuation coefficients because it is almost always lower than the corner frequency f_0 for all earthquakes studies, and the frequency is above, or equal to, the natural frequency of the typical weak-motion instruments used to record the bulk of the data used herein.
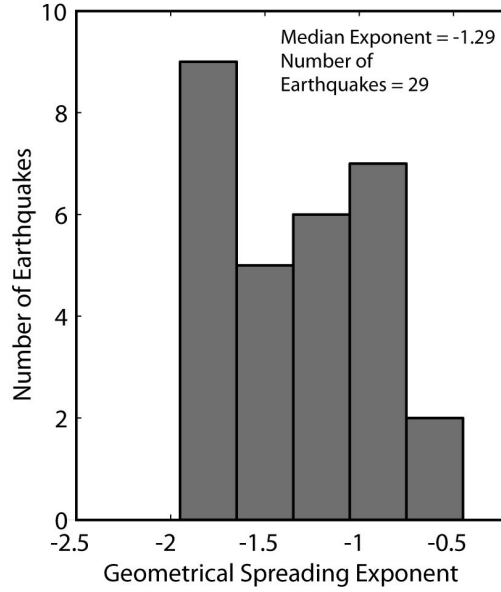
Figure 3: *Histogram of within-event geometrical attenuation at 2 Hz. Only earthquakes with three stations at hypocentral distances less than 100 km from the earthquake source are used. One station must also be at a hypocentral distance less than 50 km.*

Equipped with the provisional near-source geometrical attenuation factor *b'*, the dataset was normalized for further analysis. The first goal was to estimate an approximate source spectrum for each event with which to normalise each station over the full wave path. The normalising spectra, $A_{0,i}(f)$ is calculated by averaging $A_{ik}(f)$, corrected for geometrical attenuation, over the number of stations N_{ik} following:

$$\log A_{0,i}(f) = (1/N_{ik})\sum_{k=1}^{N_{ik}}\left[\log A_{ik}(f) - b'\log R_{ik}\right] \tag{2}$$

for all *k* such that $R_{ik} \leq 100$ km and $N_{ik} \geq 3$. This procedure is performed assuming that low frequencies are relatively unaffected by anelastic attenuation and scattering at short source-receiver distances ($R \leq 100$ km). Data from each station *j* over all *R* are subsequently normalised following:

$$\log A_{n,ij}(f) = \log A_{ij}(f) - \log A_{0,i}(f) \tag{3}$$

where $A_{n,ij}$ is the normalized spectral amplitude for earthquake *i* at the *j*th site. These normalised data are subsequently used for further analysis and revision of the Allen *et al.* (2007) source and attenuation parameters used to underpin the stochastic model.

Determination of Modelling Parameters

Over recent years, knowledge of source and attenuation parameters for southeastern Australian earthquakes has been significantly enhanced from empirical analysis of observed ground-motion data (Allen *et al.*, 2004; Allen and Atkinson, 2007; Allen *et al.*, 2007). Using new data and methods, the parameters provided in the aforementioned manuscripts are updated and their revision is discussed below. Also discussed are the aleatory uncertainties (owing to natural randomness in earthquake processes) for the parameters, which are critical for the stochastic process. All of the parameters below were determined from vertical-component ground-motions. While most of the records are on rock sites, the vertical-component motions were considered less susceptible to site effects than horizontal motions, and thus would provide more reliable source and attenuation parameters.

GEOMETRICAL ATTENUATION

It is commonly observed in intraplate regions that the attenuation of the low-frequency spectrum with hypocentral distance can be described by a tri-linear geometrical attenuation curve (Burger *et al.*, 1987; Atkinson, 2004; Edwards *et al.*, 2008). In Australia, Allen *et al.* (2007) modelled amplitude decay of low-frequency spectra to be $R^{-1.3}$ for $R \leq 90$ km. Geometrical attenuation coefficients with gradients steeper than -1 (i.e. up to $R^{-1.3}$) are also empirically observed for sites $R \leq 70$ km in ENA (Atkinson, 2004). Numerical simulations suggest that the near-source geometrical attenuation can be $R^{-1.3}$ or greater (Chapman and Godbee, 2010; 2012). While the aforementioned studies suggest higher attenuation for vertical motions than for horizontal motions is possible, empirical evidence for SEA suggests this effect is minor (e.g., Allen *et al.*, 2007), and the average difference in attenuation is accommodated in the horizontal-to-vertical (H/V) amplification model for each frequency to be discussed later.

In SEA, this rate of attenuation is observed to a transition zone in which direct waves are joined by postcritical reflections from the Moho. In this transition zone, a slight amplification in ground-motion was observed to a distance of approximately 160 km. Beyond 160 km, Allen *et al.* (2007) modelled the low-frequency spectrum to attenuate as $R^{-1.6}$. The high attenuation observed in SEA beyond the transition zone is due to the broad crustal velocity gradient (Collins *et al.*, 2003) that allows dispersion of *Lg*-wave energy into the upper mantle (e.g., Bowman and Kennett, 1991; Atkinson and Mereu, 1992).

The normalized Fourier spectra at 2 Hz are plotted for all earthquakes that have at least three stations at distances $R \leq 100$ km. These observations are subsequently binned in one-tenth log units and the median values computed. The Nelder-Mead technique is used to optimize the L2 objective function for a piecewise tri-linear geometrical attenuation function to the median amplitudes (Fig. 4). The geometrical attenuation curve $G(R)$ derived for SEA in the present study can be represented by:

$$\log G(R) = \begin{cases} b_1 \log R & R \leq R_1 \text{ km} \\ b_1 \log R_1 + b_2 \log(R/R_1) & R_1 < R \leq R_2 \text{ km}. \\ b_1 \log R_1 + b_2 \log(R_2/R_1) + b_3 \log(R/R_2) & R > R_2 \text{ km} \end{cases} \quad (4)$$

Comparisons of the coefficients b_1, b_2, b_3, R_1, and R_2 from the present study and those of Allen *et al.* (2007) are provided in Table 3. While the differences between the geometrical attenuation functions developed herein are relatively minor compared to those presented in Allen *et al.* (2007), the differences observed at distances beyond 90 km are significant and these effects should be considered for subsequent analysis.
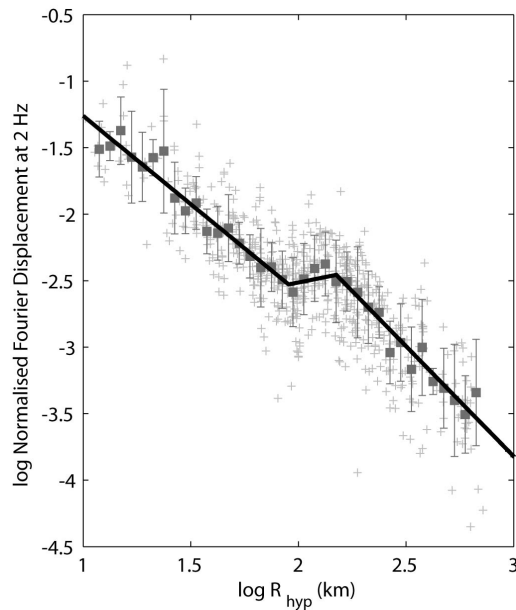
Figure 4: *The geometrical attenuation curve G(R) derived for SEA. Normalised individual 2 Hz amplitude data (grey crosses) are binned by distance in 0.05 logarithmically spaced windows. The median normalised amplitude in each bin is indicated by the solid grey squares. These median values are in turn optimised to find the best fit for a tri-linear geometrical attenuation function as represented by Equation 4 and Table 3.*

Table 3: *Comparison of geometrical attenuation coefficients described in Equation 4 from the Allen et al. (2007) and present study. Coefficients from the present study were obtained from source-normalised Fourier displacement spectra at 2 Hz.*

COEFFICIENT	ALLEN *et al.* (2007)	PRESENT STUDY
b_1	-1.3	-1.33
b_2	0.1	0.32
b_3	-1.6	-1.66
R_1 (km)	90	90
R_2 (km)	160	150

ANELASTIC ATTENUATION

Elastic waves that propagate through the earth are attenuated by geometrical attenuation, and absorption through anelastic and scattering processes. Anelastic attenuation is the loss of elastic seismic energy through internal friction (i.e., the fracturing and/or permanent deformation of rock, and generation of heat). In contrast, scattering is defined as the dispersion and/or mode conversion of seismic energy due to transmission path heterogeneities (Dainty, 1981). The associated attenuation factor that compensates for anelastic attenuation and scattering is the seismic quality factor Q, which is an intrinsic property of the media through which seismic waves pass. The quality factor summarises the characteristics that cause loss of energy with distance for reasons other than geometrical attenuation (Wilkie and Gibson, 1995). For simplicity, the combined effects of anelastic attenuation and scattering are hereafter referred to as anelastic attenuation only (e.g., Campbell, 2009).

Since the geometrical attenuation parameters (Equation 4) are chosen to model the attenuation of low-frequency seismic energy, these parameters implicitly incorporate some anelastic attenuation effects. While this philosophy may disagree with classical theory of body-waves attenuating at a rate of $R^{-1.0}$ (e.g., Hanks and Wyss, 1972; Herrmann and Kijko, 1983), it provides a practical means to empirically model observed ground motions and has been adopted in other ground-motion modelling studies. In SEA, Allen *et al.* (2007) observed that at low frequencies ($f < 2$ Hz), Q values are consistently high. Consequently, the associated Q model recommended by Allen *et al.* (2007) is given

by $Q(f) = 363f^{0.48}$ with a minimum Q value of 1000. In effect, this implies that all attenuation at low frequencies is captured by the geometrical attenuation model and anelastic effects across the full distance range considered (i.e., for $R \leq 400$ km) can largely be ignored (e.g., Ambraseys *et al.*, 2005). It is important to note that the geometrical attenuation and anelastic attenuation models are highly correlated. Consequently, it is only valid to infer differences in attenuation between regions through the seismic quality factor if the Q models are determined from a consistent geometrical attenuation model.

Allen *et al.* (2007) compute the quality factor at each frequency assuming $Q^{-1}(f) \propto \ln A_{g,ij}(f)/R$ (see Equation 1), where $A_{g,ij}(f)$ is the normalized Fourier displacement spectra corrected for geometrical attenuation according to the equation:

$$\log A_{g,ij}(f, R_{ij}) = \log A_{n,ij}(f) - \log G(R_{ij}). \tag{5}$$

Consequently, Q at each frequency can easily be obtained through regression of the natural logarithm of normalized Fourier displacement spectra and distance (Fig. 5). While this is an effective method to determine the seismic quality factor, it can be readily observed from the results of Allen *et al.* (2007) that a linear fit between $\ln A_{g,ij}(f)$ and R is unsatisfactory and leads to an overestimation of spectral amplitudes at hypocentral distances approximately less than R_1. It is proposed that the use of the $R^{-1.3}$ geometrical attenuation at near-source distances (Equation 4) is sufficient to compensate for all attenuation effects of direct body-waves at distances less than the geometrical attenuation transition distance R_1 (approximately 90 km). Consequently, rather than apply the standard theoretical Q model as incorporated in Equation 1, anelastic effects are empirically modelled at each frequency according to the following equation (Fig. 5):

$$\ln A_{q,ij}(f, R) = \ln A_{g,ij}(f) - q(f)\sqrt[3]{R_{ij}^3 + R_1^3}. \tag{6}$$

where $A_{q,ij}(f)$ is the normalized Fourier displacement spectra, corrected for both geometrical and anelastic attenuation. The frequency dependence of the coefficient q is indicated in Figure 6. For frequencies 2.0-24 Hz, q can be approximated using the equation:

$$q(f) = 5.85 \times 10^{-3} - 0.015 \log f \quad \text{for } 2 \leq f \leq 24 \, \text{Hz} \tag{7}$$

The variability of q at frequencies less than approximately 1 Hz is thought to be due to limitations of the short-period instruments used to record the data. Consequently, values of q for $f \leq 2$ Hz are set to zero for further analysis. Figure 7 shows the application of the anelastic attenuation model proposed above. This method is similar to the attenuation models recently promoted by Morozov (2008; 2009), who argues that attenuation models need not rely on elaborate theoretical models or restrictive assumptions and can be guided by the data. It is observed that the proposed anelastic attenuation model presented herein performs well across the full frequency and distance range of the data considered (Fig. 7).
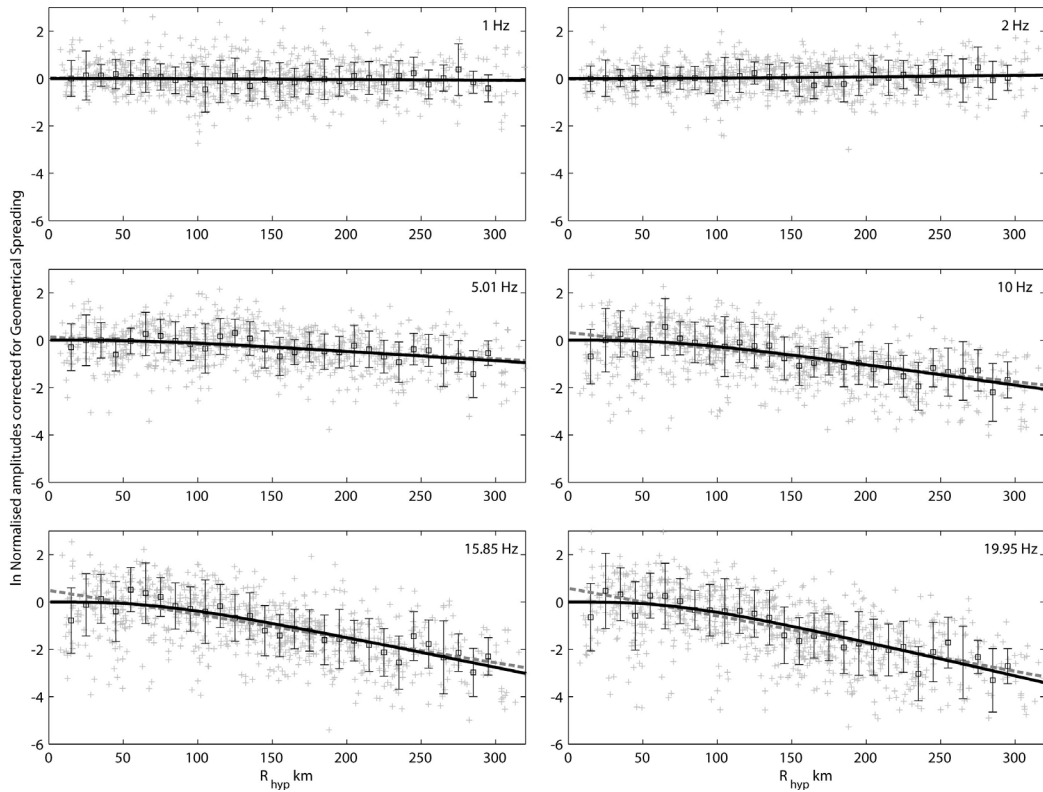
Figure 5: Normalized 2 Hz Fourier displacement spectra corrected for geometrical attenuation and plotted against R for a suite of six spectral frequencies from 1-20 Hz. Individual amplitude data (grey crosses) are binned by distance in linearly-spaced 10-km windows. The median normalised amplitude in each bin is indicated by the black squares. The decay of normalised spectral amplitudes represents attenuation through anelastic and scattering effects. The grey dashed line is proportional to the traditional seismic quality factor, where $Q^{-1}(f) \propto \ln A_{g,ij}(f)/R$ (see Equation 1). These data suggest that using such a functional form might lead to an overcorrection of near-source spectral amplitudes by almost a factor of two in ground-motion, particularly at high frequencies. The solid black line empirically models the anelastic effects at each frequency according to Equations 6 and 7.
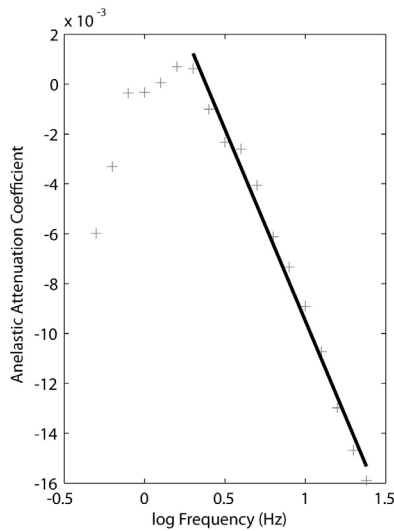
Figure 6: The anelastic attenuation coefficient, q(f), indicating the change in the rate of anelastic attenuation with frequency (see Equations 6 and 7). The downward trend at low-frequencies is thought to be due to low-quality data at frequencies less than approximately 1 Hz. These frequencies are generally below the natural frequency of the seismometer and are poorly resolved.
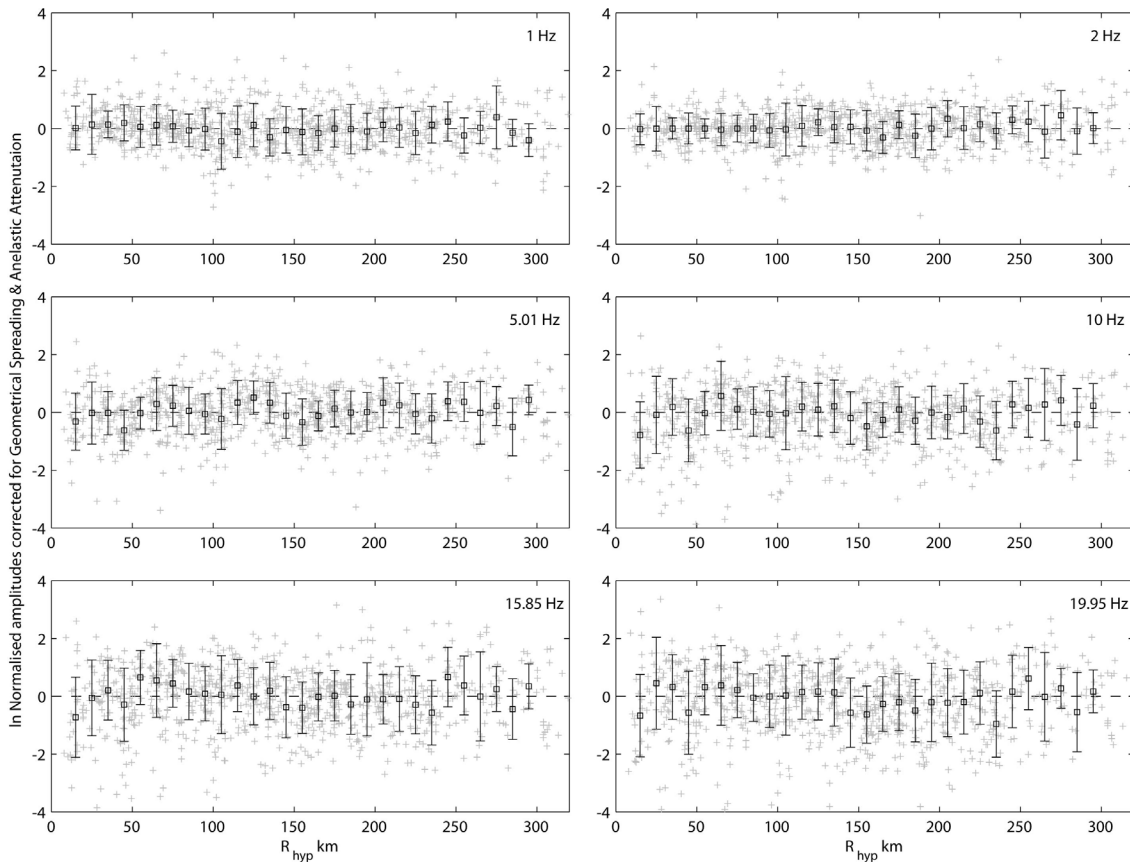
Figure 7: Normalised 2 Hz Fourier displacement spectra corrected for both geometrical attenuation and anelastic attenuation, plotted against R for a suite of six spectral frequencies from 1-20 Hz. Individual amplitude data (grey crosses) are binned by distance in linearly-spaced 10-km windows. The median normalised amplitude in each bin is indicated by the black squares. Error bars indicate the standard deviation of residuals for each distance window. The zero dashed line is relative to the median of the combined individual corrected amplitude data for each frequency.

KAPPA

Several recent studies have made significant progress in understanding the characteristics of the path-independent site diminution parameter kappa, κ_0 (Anderson and Hough, 1984; Hough *et al.*, 1988), and its relationship with near-surface shear-wave velocity in stable continental regions (Chandler *et al.*, 2006; Campbell, 2009; Douglas *et al.*, 2010; Drouet *et al.*, 2010; Edwards *et al.*, 2011). The kappa parameter is a critical component in stochastic ground-motion modelling and controls the high-frequency segment (and peak ground acceleration) of the response spectrum. The zero subscript refers to kappa estimated from acceleration spectra corrected for anelastic attenuation such that the near-source shape of each record is resolved (e.g., Atkinson, 1996).

Prior empirical studies in Australia sought only to model observed ground-motions through empirical regressions (e.g., Allen *et al.*, 2007) and did not attempt to isolate the effect of κ_0. Consequently, in order to forward model displacement spectra employing Equation 1, a regional value of κ_0 for southeastern Australia must be determined. Recent studies indicate that near-surface effects, as modelled with κ_0, may be stronger in the upper crust of SEA than in ENA (Allen and Atkinson, 2007). However, the comparison of modelled vertical-component Fourier displacement spectra developed for SEA (Allen *et al.*, 2007) and ENA (Atkinson, 2004) at short hypocentral distances show no such discrepancy at high frequencies (shown in Allen *et al.*, 2007). In contrast, these differences may reflect random earthquake effects in the limited magnitudes and narrow distance range of the data considered for the particular comparison made by Allen and Atkinson (2007).

Herein, we evaluate an average value for κ_0 using vertical-component ground-motion records corrected for anelastic attenuation effects, following:

$$\ln a_{\kappa,ij}(f,R) = \ln\left[(2\pi f)^2 A_{ij}(f)\right] - \min[q(f),0]\sqrt[3]{R_{ij}^3 + R_1^3} \,. \tag{8}$$

where $a_{\kappa,ij}(f)$ is the normalised acceleration spectra. In the present study, geometrical attenuation is treated as being frequency-independent. Consequently, following the correction for anelastic effects, the remaining contributions to change in the high-frequency spectral shape is attributed only to κ_0. Anelastic attenuation corrected spectra are then aggregated by station j and each spectrum is normalised by the Fourier acceleration amplitude at 2 Hz. Kappa is subsequently determined for each site j by linear least squares regression between the natural logarithm of acceleration spectra and frequency between 12 and 20 Hz [e.g., $\kappa_{0,j} \propto \ln a_{\kappa,ij}/f$ (see Equation 1)]. Despite variations in f_0 for different sized events, the site dependent decay from the theoretical ω^2 [$= (2\pi f)^2$] acceleration source model (Brune, 1970) should remain constant and is indicative of κ_0 (Figure 8). The minimum regression frequency of 12 Hz is also beyond the theoretical range of each earthquake's corner frequency. In these calculations, a magnitude-distance criterion is imposed to only include data for earthquakes larger than moment magnitude M_W 3.5, recorded at distances less than 250 km and for stations with three or more records. In these analyses, a negative kappa value was resolved for some stations. This observation has also been noted in other studies (Drouet *et al.*, 2010; Edwards *et al.*, 2011). The negative kappa values determined in the present study reflects the inherant variability in the attenuation modelling and the fact that a mean anelastic attenuation model – which overwhelmingly affects the high-frequency spectrum – may not accurately reflect the attenuation characteristics of each source-to-site path in the dataset, or the amplification characteristics of the crust underlying the site. Consequently, over-correction to the high-frequency spectral shape from the anelastic parameters may violate the assumption of the Brune (1970) ω^2 source model and may require correction to the theoretical spectral shape. Furthermore, κ_0 is highly sensitive to variations in both the anelastic attenuation model used, coupled with the frequency band in which the regression is performed (e.g., Drouet *et al.*, 2010). In the present analysis, the step-wise inversion process allows us to decouple path and site parameters prior to the assessment of κ_0.

Figure 9 shows a histogram of the calculated κ_0 values for the 71 sites that are consistent with the magnitude-distance and record number (three or more) criteria. This indicates a normal distribution with a mean kappa value of 0.006 ± 0.017 s. This median kappa value is similar to that recommended (0.006 s) for central and eastern North America (e.g., Electric Power Research Institute, 2003; Hashash *et al.*, 2011) and that used (0.005 s) by Atkinson and Boore (2006) and Campbell (2009) for the same region. However, this value is explicitly tied to suite of stochastic parameters presented herein and cannot be considered in isolation.

Rather than simply being a modelling parameter, as assumed herein, it is suggested that kappa is a real physical variable and should be treated as such (Ken Campbell, pers. comm., 2012). Consequently, the abundance of negative κ_0 values as calculated here (Fig. 9) may seem counter-intuitive to the broader geotechnical and ground-motion modelling community. Edwards *et al.* (2011) suggested that the evaluation of negative κ_0 values may potentially be due to the effect of site-specific amplification or resonance features being reflected in κ_0.
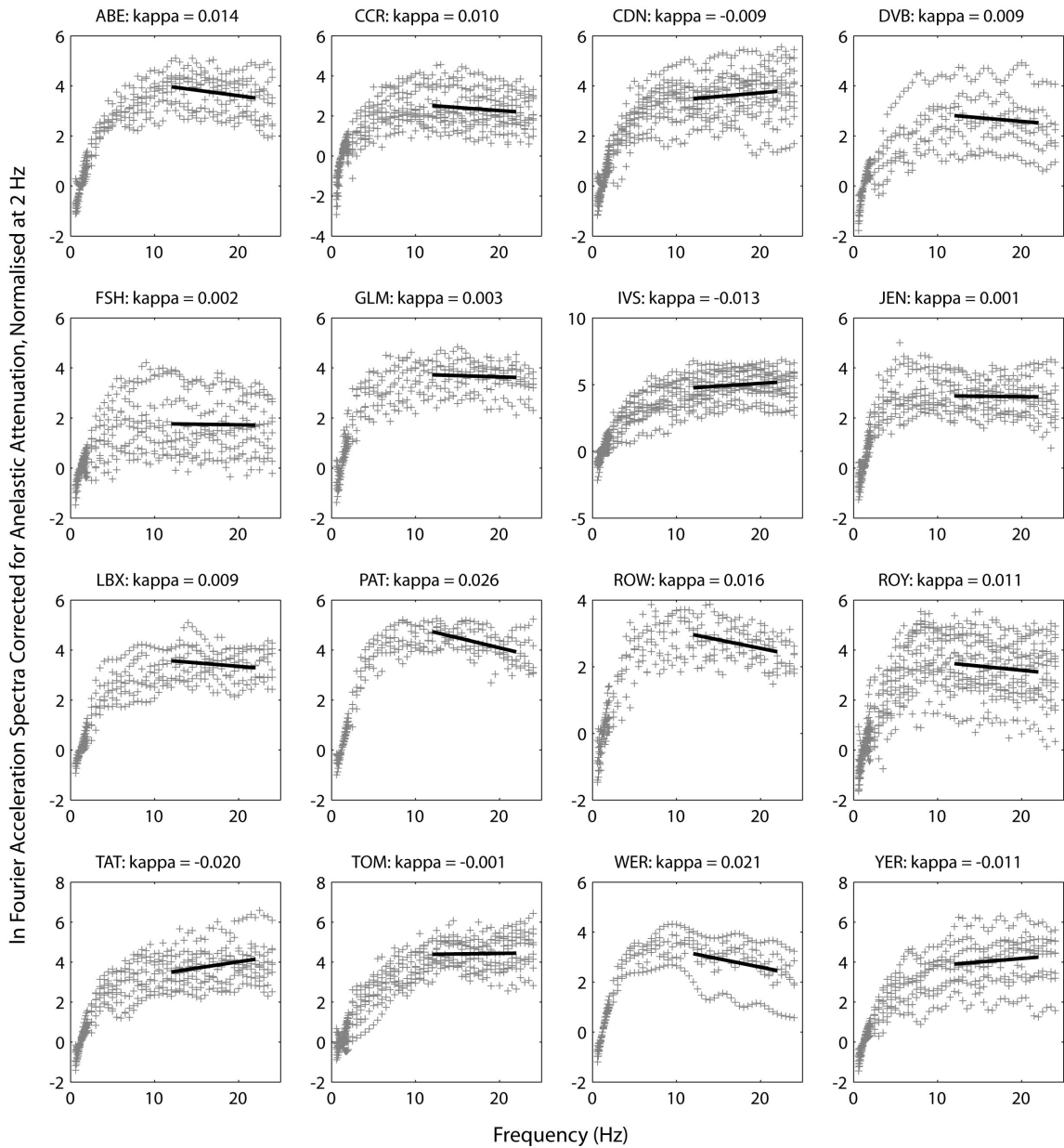
Figure 8: *Examples of κ0 calculation for representative stations in southeastern Australia. Vertical-component Fourier spectra corrected for the effects of anelastic attenuation are then aggregated by station and each spectrum is normalised by the Fourier acceleration amplitude at 2 Hz (grey crosses). Kappa is subsequently determined for each site by linear least squares regression between the natural logarithm of acceleration spectra and frequency between 12 and 20 Hz (solid black lines).*
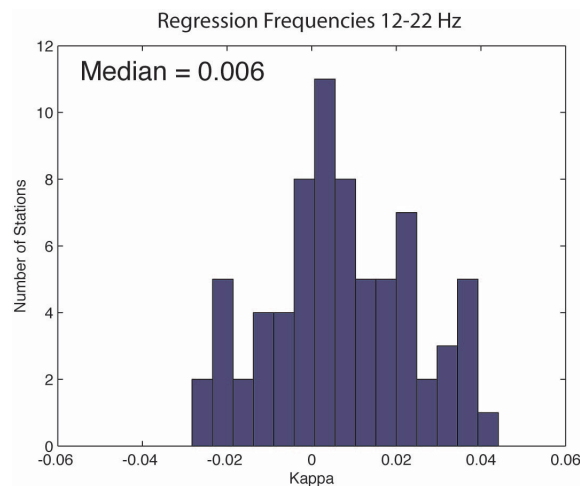
Figure 9: Histogram of the calculated κ0 values for the 71 sites that are consistent with the magnitude-distance and record number (three or more) criteria. In this study, negative κ0 values are allowed and are interpreted to reflect that the mean anelastic attenuation model – which may not accurately reflect the attenuation characteristics of each source-to-site path in the dataset – absorbs some of the kappa effect.

To examine this question in more detail, it is expected that average kappa values as calculated herein would normally be associated with a V_{S30} of 2,000 m/s and higher (e.g., Van Houtte *et al.*, 2011). However, based on the limited V_{S30} data collected in Australia, it is clear that average V_{S30} values are not in this velocity range (Collins *et al.*, 2006; Kayen and Carkin, 2006; Kayen *et al.*, 2010). In order to reconcile the apparent discrepancy between the Australian data, and other stable continent data, intra-site kappa residuals (mean site kappa minus kappa from individual records) are determined for each seismic station and aggregated for the complete dataset.

Because the kappa value is dependent on the high-frequency acceleration spectrum, it is sensitive to the anelastic attenuation factors, as described above. To determine whether these anelastic attenuation parameters bias the calculated κ_0 to values smaller than expected, the intra-site residuals are plotted against distance (Fig. 10). Because the anelastic attenuation parameters used herein apply little-to-no correction at distances less than R_1 (less than 90 km), the shape should not be affected by any kappa biases due to over-correction of anelastic effects at short distances. Consequently, the shape of the acceleration spectrum (at $f > f_0$) should be representative of the earthquake source spectrum combined with the kappa effect. Any deviation of intra-site κ_0 values with hypocentral distance should reveal whether the assumed anelastic attenuation is appropriate. As can be seen from Figure 10, there is limited departure from zero for the median intra-site residuals across the full distance range. While the first few data points suggest that higher kappa values might be appropriate, the median residuals are based on relatively few data. From 40 to 90 km, where no effective anelastic correction is applied, the median residuals are near zero. Beyond this distance range, the residuals do not deviate significantly from zero.

The correlation between kappa and V_{S30} is discussed in more detail in the section 'Definition of an "Average Rock" Site' below.
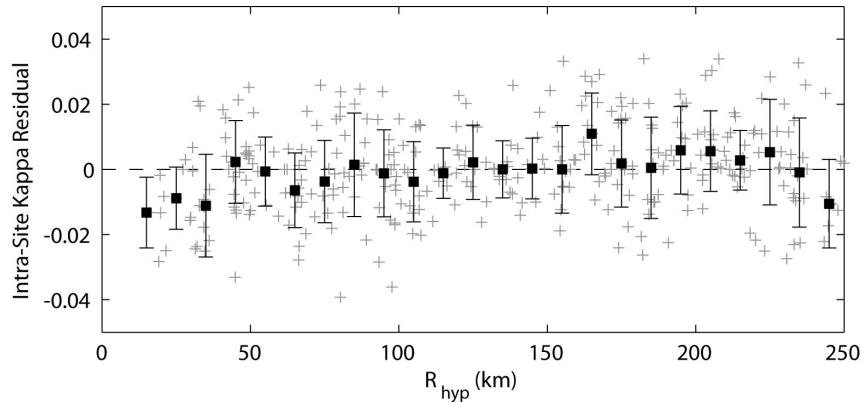
Figure 10: *Intra-site kappa residuals (mean site kappa minus kappa from individual records) against hypocentral distance. Individual residuals (grey crosses) are binned in 10-km windows and the median and standard deviation calculated (black squares). The figure shows limited departure of the median values from zero over the distance range considered.*

MOMENT MAGNITUDE

With the attenuation coefficients evaluated above, earthquake source parameters can now be determined. The Fourier displacement source spectra $A_i(f)$ can be estimated for each earthquake i by taking the mean of the individual spectra corrected for attenuation effects, following:

$$\ln A_i(f) = (1/N_i) \sum_{j=1}^{N_i} \left[\ln\left[A_{ij}(f)/G(R_{ij})\right] - \min\left[q(f),0\right] \sqrt[3]{R_{ij}^3 + R_1^3} + \pi f \kappa_{0,j} \right] \tag{9}$$

where N_i is the number of recordings for each earthquake and $\kappa_0 j$ is the site-dependant kappa coefficient. For records that do not have a station specific $\kappa_0 j$, the median kappa value of 0.006 is used.

For each earthquake, the low-frequency spectral level, Ω_0, is calculated from the low-frequency segment of the average displacement source spectrum $A_i(f)$ for frequencies less than f_0. The frequency range of the calculation was manually picked for each earthquake by the author. Examples of the average source spectrum, superimposed on individual source-corrected spectra for several representative earthquakes are shown in Figure 11. Seismic moment M_0 is then calculated following:

$$M_0 = \Omega_0/C \tag{10}$$

where M_0 is in N-m and the values of ρ = 2,800 kg/m^3 and β = 3,600 m/s from the coefficient C defined above in Equation 1. Moment magnitude M_W can subsequently be calculated using the equation (Hanks and Kanamori, 1979).

$$M_W = \frac{2}{3} \log M_0 - 6.03 \tag{11}$$

Moment magnitude estimates using the updated attenuation parameters determined herein are largely consistent with those magnitudes from Allen *et al.* (2007) for the events in common. On average, a slight reduction in M_W of less than 0.01 magnitude units is observed in using the revised attenuation parameters. Moment magnitudes used for further analysis for all earthquakes are provided in Table 1.
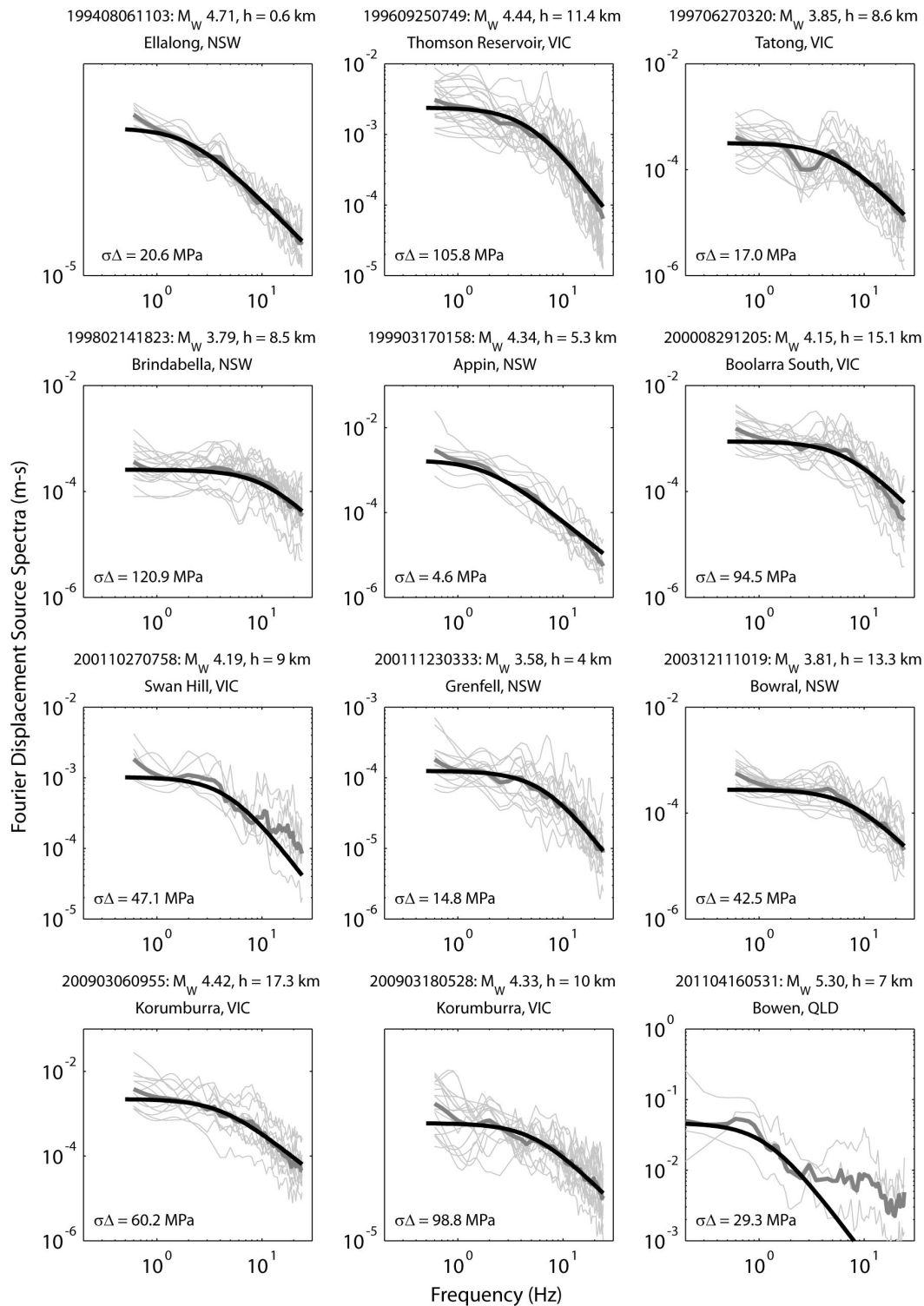
Figure 11: *The average source spectrum (thick grey line), superimposed on individual source-corrected spectra (thin grey lines), for several representative earthquakes. The theoretical Brune source spectrum is superimposed in each subplot (thick black line). The calculated Brune stress drop for each earthquake is indicated in the bottom-left of each subplot.*

BRUNE STRESS DROP

The Brune stress drop $\Delta\sigma$ parameter is another key input into stochastic modelling processes, and one that carries a high degree of uncertainty. Estimates of Brune stress drop are also sensitive to other

parameters in the inversion process; in particular the attenuation model as well as M_0 and κ_0 (Boore *et al.*, 1992; Boore *et al.*, 2010; Boore, 2012). This is the key reason the author has chosen to undertake a step-by-step inversion process to isolate individual parameters rather than a joint inversion of all source and/or attenuation coefficients. Following the logical framework outlined thus far ensures there are no trade-offs in the determination of key parameters.

It is generally agreed that earthquakes in intraplate regions, such as Australia, result in higher average Brune stress drops than those earthquakes in active tectonic regions (Kanamori and Anderson, 1975; Scholz *et al.*, 1986; Boore and Atkinson, 1987; Allmann and Shearer, 2009). However, it is important to first define what is meant by the term "intraplate". Scholz *et al.*, (1986) define intraplate regions as those regions that are located far from any known plate boundary. Intraplate earthquakes can be further subdivided into those that occur in a diffuse zone related to plate-boundary deformation and those that are true mid-plate, or stable continental region events. Based on the fault scaling relations of Somerville *et al.* (2001) and slip models generated for the Meckering and Tennant Creek earthquakes (Somerville *et al.*, 2009), rupture areas of earthquakes in cratonic Australia are assumed to be approximately half those of non-cratonic earthquakes. This finding is consistent with high average stress drops for stable continental earthquakes. This is because fault asperities in stable regions generally possess higher frictional strength than in active regions (Scholz *et al.*, 1986) and thus require higher stress to overcome the rigidity of the rocks in the crust. Several recent studies have estimated $\Delta\sigma$ for earthquakes in stable continental regions (Allen *et al.*, 2004; Allen *et al.*, 2006; Edwards *et al.*, 2008; Boore *et al.*, 2010; Drouet *et al.*, 2010). While significant advances in estimating $\Delta\sigma$ for earthquakes in several stable continental regions have been made, comparisons of Brune stress drops between regions cannot be meaningfully compared unless the attenuation model is also considered (Boore *et al.*, 2010).

Armed with revised estimates of M_0 for each event, a Brune (1970) ω^{-2} source model is fitted to the average source spectra $A_{0,i}(f)$ for each event to invert for the corner frequency f_0. The source follows the general form:

$$A(M_0, f) = \frac{CM_0}{\left[1 + (f/f_0)^2\right]} \tag{12}$$

The Brune stress drop is subsequently estimated following:

$$\Delta\sigma = \frac{7}{16}\frac{M_0}{r_0^3} \tag{13}$$

where $r_0 = 2.34\,\beta\,/\,(2\pi f_0)$ is the radius of a circular fault (Brune, 1970; 1971) The fit of the Brune ω^2 source model on the average source spectra was optimized for a magnitude-dependent frequency range, which was focussed on capturing the best estimate of corner frequency (Figure 11). Because the optimization of the Brune model did not yield satisfactory estimates of f_0 and $\Delta\sigma$ for all earthquakes, the misfit between the theoretical source model and the average source spectra $A_{0,i}(f)$ (in log space) was used to ensure only the best estimates of $\Delta\sigma$ were considered for the stochastic modelling. The preferred estimates of stress drop were determined by calculating the standard deviation of the residuals over a magnitude-dependent frequency range, indicated below:

$1.5 \leq f \leq 22$ Hz for $M_W < 4.0$

$0.8 \leq f \leq 10$ Hz for $4.0 \leq M_W < 4.8$ (14)

$0.5 \leq f \leq 2.5$ Hz for $M_W \geq 4.8$

Brune stress drops for those earthquakes with a log standard deviation of residuals less than 0.07 are indicated in Table 2. The geometric mean of $\Delta\sigma$ is 31 MPa (± 0.37 log MPa) for all earthquakes.

The notion of stress drop varying with either magnitude or hypocentral depth is a question that remains unresolved. In their comprehensive assessment of stress drop from global earthquakes, Allmann and Shearer (2009) found no evidence to support variable stress drop with earthquake magnitude. However, their study only considered earthquakes of (moderate) magnitudes M_W 5.2 and above. Several studies have shown a departure from self-similar source scaling indicating decreasing Brune stress drops for small-magnitude earthquakes M_W 4.0 and below (Bungum et al., 1982; Nuttli, 1983; Atkinson, 1993; Shi et al., 1998; Drouet et al., 2010). However, other researchers have suggested the apparent breakdown at low magnitudes is simply an artefact of severe attenuation of the high-frequency energy obscuring the corner frequency in the upper few kilometres of the crust (Abercrombie and Leary, 1993; Abercrombie, 1995). The phenomenon of decreasing Brune stress drop has also been observed for small earthquakes in both eastern (Allen et al., 2004) and western (Allen et al., 2006) Australia. However, the latter dataset in Western Australia consisted largely of recordings from a single earthquake sequence. Consequently, it is suggested the very low Brune stress drops observed for some of these low magnitude events is because they were aftershocks occurring on recently-ruptured surfaces (Allen et al., 2006). Brune stress drops from the study in Western Australia may therefore not provide support to the breakdown of self-similarity for low-magnitude earthquakes.

With the revised Brune stress drops for SEA earthquakes, the variation between stress and magnitude is investigated. Figure 12a shows the variation $\Delta\sigma$ with M_W, which indicates an increasing trend in $\Delta\sigma$ with M_W. However, because of the limited magnitude range of the dataset, it cannot be concluded that this Brune stress drop increase continues with magnitude. In contrast, the highest moment magnitudes in the dataset indicate a slight decrease in $\Delta\sigma$ with M_W. Considering sparse data at higher magnitudes, it does appear that $\Delta\sigma$ may become self-similar at magnitudes $M_W > 4.0$ as suggested by Atkinson (1996).

An alternative hypothesis is that Brune stress drop vary with hypocentral depth, h, because of an increase of crustal stresses at greater depths (e.g., Haimson, 1978). Additionally earthquakes at shallow depths may be indicative of slower rupture velocities which would result in lower stress drops (Allmann and Shearer, 2007). This phenomenon has been previously observed in SEA (Allen et al., 2004) and elsewhere (Allmann and Shearer, 2007). Several authors have observed systematic variations in the relative occurrence of small-to-large earthquakes (i.e., the b-value) (Mori and Abercrombie, 1997; Gerstenberger et al., 2001; Allen et al., 2004), which is thought to be due to the increasing crustal stress levels with depth. Furthermore, it is observed from both mining-triggered and natural seismicity that the b-value is inversely proportional to stress (Urbancic et al., 1992; Schorlemmer et al., 2005) – that is, fewer small earthquakes are indicative of high in situ stress. Consequently, the apparent increase in Brune stress drop with earthquake magnitude may be an artefact of low-magnitude earthquakes more commonly occurring at shallow depths in lower stress environments.

With the updated earthquake source parameters and augmented earthquake ground-motion database, this observation in SEA is reviewed. Using only the best quality Brune stress drop estimates, $\Delta\sigma$ is plotted against h (Figure 12b). These data suggest that there is a significant differentiation between $\Delta\sigma$ for earthquakes at a depth of approximately $h = 10$ km, with shallow earthquakes having consistently lower values of $\Delta\sigma$ than deeper events. Notable examples of low Brune stress drop estimates for shallow earthquakes are the moderate magnitude 1994 M_W 4.7 Ellalong and 1999 M_W 4.3 Appin earthquakes (see Table 2 and Fig. 11). Rather than a continuous variation, the change in $\Delta\sigma$ with depth, there appears to be a discrete step from relatively low-to-high $\Delta\sigma$ with increasing depth. However, it should be noted that we do not expect stress drops to continue

to increase with increasing depth due to thermal gradients in the crust, which control the seismogenic depth in continental crust.
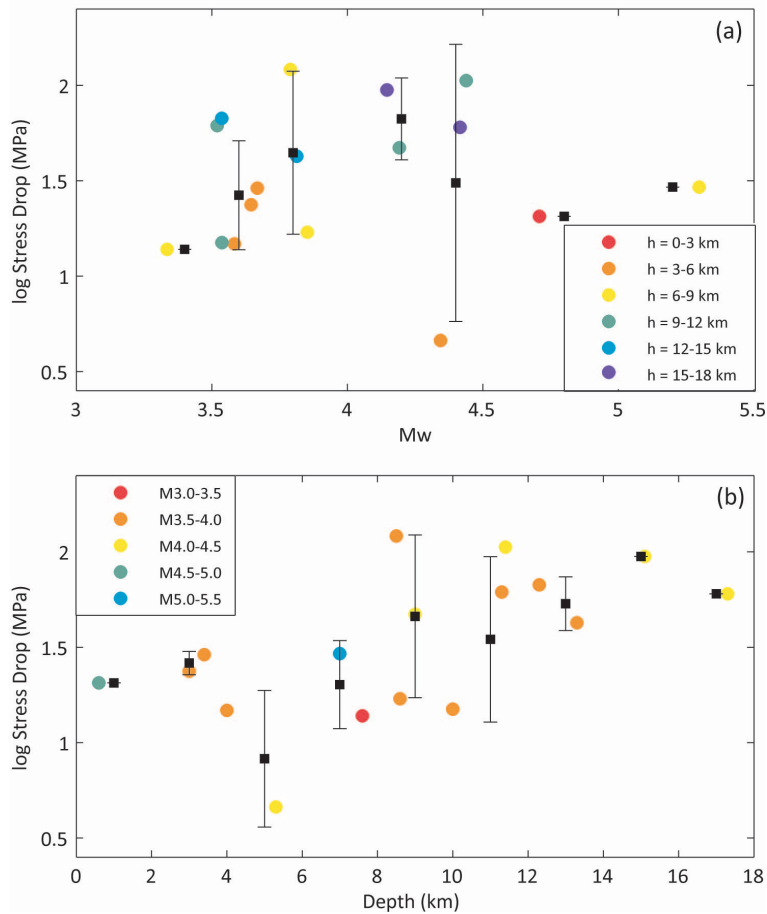
Figure 12: *(a) The variation $\Delta\sigma$ with M_W. Brune stress drops for individual events are colour-coded by depth, h. Solid black squares indicate the mean stress drop and its standard deviation for each 0.2 magnitude unit window. (b) The variation $\Delta\sigma$ with depth. Brune stress drops for individual events are colour-coded by M_W. Solid black squares indicate the mean stress drop and its standard deviation for each 2 km depth bin.*

Given the apparent differences in $\Delta\sigma$ with h, a single GMPE may not be appropriate to represent ground-motions from earthquakes in SEA. It is suggested that GMPEs be developed for both shallow and deep earthquakes. Consequently, the average Brune stress drop is calculated for shallow and deep events. The geometric mean of Brune stress drop is 23 MPa and 50 MPa ($\pm$ 0.31 log MPa) for shallow and deep events, respectively. While these values might appear higher than what is considered normal (e.g., Allmann and Shearer, 2009), they are similar with recent studies in ENA (Boore *et al.*, 2010; Boore, 2012) and internally consistent with the attenuation parameters derived herein.

DURATION OF MOTION

The duration T of an earthquake coda at a hypocentral distance R is generally represented as:

$$T(R) = T_0 + dR, \tag{15}$$

where T_0 (= $1/f_0$) is the source duration and d is the coefficient that controls the increase of duration with distance (Atkinson and Boore, 1995). Each velocity time-history was band-pass filtered between frequencies $0.707\,fn \le fn \le 1.414\,fn$ using a fourth-order Butterworth filter, where fn represents a suite of frequencies between 2 and 10 Hz (e.g., Raoof $et\ al.$, 1999). The filtered time histories were then squared and integrated over time. The integration begins at the S-wave arrival and continues into the coda until an energy plateau is reached (e.g., Bay $et\ al.$, 2003). Because many of the seismograms are not continuous recordings, the S-wave coda can often be incomplete for the purposes of estimating duration of ground shaking. Consequently, a if the integral varied by more than 2% of the total integral in the final two seconds of the time-history, the record was rejected for further analysis. In the present study, the duration $T(R)$ was estimated as the time window within which the integral reaches 5-80% of its total value. The source duration T_0 was then subtracted from the coda duration to determine the distance-dependent coefficient, d.

Examination of distance-dependent duration functions indicate very subtle variations with frequency for the frequency range considered. Consequently, the duration of earthquake coda is taken as that given by the filtered time-histories about 1.0 Hz (Fig. 14). The shape of the distance-dependent tri-linear duration function is similar to that given by Atkinson and Boore (1995) for ENA. However, at larger distances the SEA coda durations are significantly less than those observed for ENA, by up to 6.5 seconds at some distances. Decreasing duration generally results in larger ground-motions because the total energy is condensed into a shorter time window (Atkinson, 1993). Using the transition distances of R_{d1} = 70 and R_{d2} = 170 km the duration function can be defined by:

$$dR = \begin{cases} d_1 R & R \le R_{d1} \\ d_1 R_{d1} + d_2(R - R_{d1}) & R_{d1} < R \le R_{d2} \\ d_1 R_{d1} + d_2(R_{d2} - R_{d1}) + d_3(R - R_{d2}) & R > R_{d2} \end{cases} \tag{16}$$

where d_1, d_2 and d_3 are 0.14, -0.04 and 0.07, respectively at distances less than 400 km. Limited empirical data beyond 300 km suggest a plateau in earthquake coda duration at larger distances. Because the GMPE defined herein is derived for distances less than 400 km, the duration model up to 300 km is extrapolated to larger distances because EXSIM cannot accommodate a more complicated functional form. This simplification is expected to have relatively minor effects on the stochastic model for ground motions of engineering significance. Note the transition distances for earthquake duration R_{d1} and R_{d2} are not to be confused with those used for the geometrical attenuation in Equation 4.
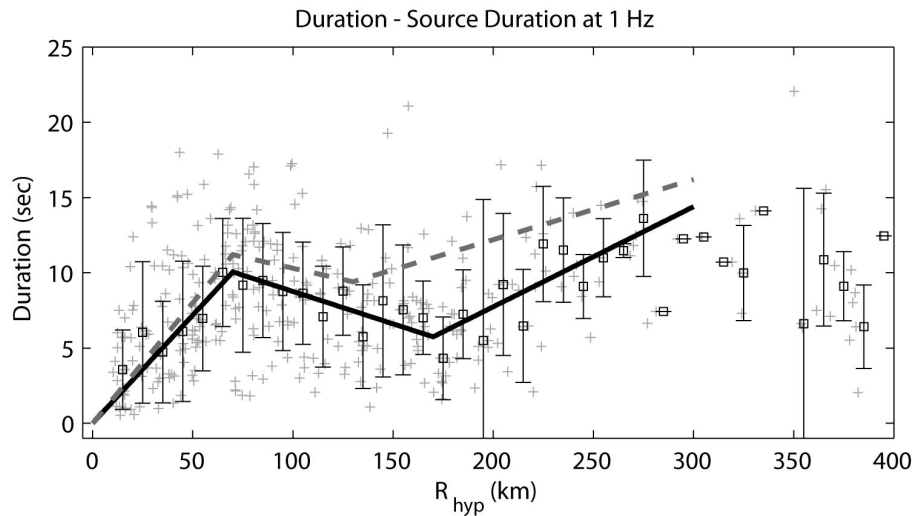
Figure 13: *Modelled duration of earthquake coda for southeastern Australian earthquakes from filtered time-histories about 1.0 Hz. The duration for each record (grey crosses) is defined as the time period through which the integral of the velocity time history reaches 5-80% of its total value from the S-phase onset, minus the source duration T_0. Individual durations were binned in 10-km windows and the mean and standard deviation for each distance window was calculated (black squares). A tri-linear duration model was then fitted to the median durations (solid black line). The shape of the Atkinson and Boore (1995) duration model for ENA is also indicated (dashed grey line). The poor resolution of the data beyond 300 km suggests the model is only applicable to approximately 300 km.*

VERTICAL-TO-HORIZONTAL AMPLIFICATIONS

The source and attenuation parameters defined above are based on the analysis of vertical-component data, which are assumed to be unaffected by site effects. Atkinson (2004) suggests that the horizontal component of motion is amplified by impedance gradients as the surface is approached, whereas this effect on the vertical component is counteracted by the refracting of rays toward the vertical in the velocity gradient for rock sites. The net effect is that there is little amplification of the vertical component, making the H/V ratio a crude approximation of the near-surface amplification for rock sites (Chen and Atkinson, 2002; Atkinson, 2004).

Since the goal herein is to develop GMPEs for the horizontal-component of response spectra for typical rock sites in SEA, it is necessary to apply a horizontal correction factor to the stochastic simulations. Atkinson and Boore (2006) used horizontal-to-vertical component ratios (H/V ratios) for hard rock sites in ENA to develop amplification factors for National Earthquake Hazards Reduction Program (NEHRP) A site conditions (Building Seismic Safety Council, 2003).

Using smoothed horizontal- and vertical-component ground motions from the SEA dataset, the average H/V ratio, which is assumed to be equivalent to the horizontal amplification factor, is determined for ground-motions between 0.4 and 25 Hz. The average ratios were smoothed using spline interpolation and are assumed to represent average rock conditions for SEA (to be discussed later). Because Fourier spectra in the empirical analysis are only used up to a frequency of 25 Hz, the amplification value at 25 Hz is extrapolated to higher frequencies for the stochastic simulations. By comparison, the amplification factors used by Atkinson and Boore (2006) for their hard-rock GMPE (NEHRP site class A) are a factor of 1.2 smaller at 5.0 Hz than for the amplification factors used for the SEA models (Table 4).

Table 4: *Site amplification factors used for typical rock sites in southeastern Australia (SEA) as used in the stochastic simulation. The amplification factors were determined from H/V ratios of recorded Fourier shear-wave spectra. The amplification factors used in the Atkinson and Boore (2006) GMPE for eastern North American rock sites are shown for comparison*

FREQUENCY (HZ)	AMPLIFICATION FACTOR	
	THIS STUDY	ATKINSON & BOORE (2006)
≤ 0.40	1.00	–
0.50	1.04	1.00
1.00	1.23	1.13
1.59	1.33	–
2.00	1.40	1.22
3.16	1.55	–
5.01	1.64	1.36
7.94	1.58	–
10.0	1.53	1.41
15.9	1.50	–
20.0	1.50	–
33.4	1.50	1.41 (at 50 Hz)
82.0	1.50	

FINAL MODELLING PARAMETERS

In the simulations to produce median ground-motion prediction equations, aleatory uncertainty is included by treating each key parameter as a probability distribution, with the given median value and variability about that median derived in the analysis above. It is assumed that the variability about the median values is approximately Gaussian for all parameters (i.e. the median and mean values are approximately equal). The standard deviation thus approximates the aleatory variability about the median values. Tables 5 and 6 provide the final modelling parameters and aleatory uncertainties to be used in the stochastic simulations for both the shallow- and deep-earthquake models.

Table 5: Mean parameter values for SEA ground-motion simulations with EXSIM for shallow- and deep-earthquake models.

PARAMETER	MEAN VALUE
Shear-wave velocity, β	3,600 m/s (Wesson, 1988)
Density, ρ	2,800 kg/m^3
Rupture propagation speed	0.8 β
Brune stress drop, $\Delta\sigma$	23 MPa (shallow model)
	50 MPa (deep model)
Pulsing percentage	25%
Geometrical attenuation R^b, b	-1.33 (0-90 km)
	+0.32 (90-150 km)
	-1.66 (> 150 km)
Anelastic attenuation, $q(f)$	min[0,5.85×10^{-3} – 0.015 log f]
κ_0	0.006 s
Distance-dependent duration	0.00 (0-10 km)
	+0.14 (10-70 km)
	-0.04 (70-160 km)
	+0.07 (> 160 km)
Fault dip	35°

Table 6: Aleatory uncertainty (variability) in key model parameters using normal distribution for shallow- and deep-earthquake models.

PARAMETER	MEAN	STANDARD DEVIATION	MINIMUM	MAXIMUM
Fault dip	35°	20°	10°	90°
$\log_{10}$ stress (MPa)	1.36 (shallow) 1.70 (deep)	0.31	1.0	3.1
κ_0 (s)	0.006	0.017	-0.010	0.024
b_1	-1.33	0.23	-1.61	-1.05
b_2	+0.32	0.28	+0.02	+0.62
Shallow model depth distribution (km)	6	6	1	12
Deep model depth distribution (km)	13	5	7	19
Fault area scaling factor	1.0	0.3	0.7	1.3

Definition of an "Average Rock" Site

Throughout this manuscript, there have been references to the term "average rock" for southeastern Australian crust. In this section, the definition of the average site is explored in more detail. Most modern GMPEs are explicitly calibrated to the time-averaged shear-wave velocity in the upper 30 m of the Earth's crust, V_{S30}. While there is still much debate as to the suitability of V_{S30} as a proxy for site amplification factors (e.g., Castellaro *et al.*, 2008), it is the most commonly used factor in modern ground-motion predictions (e.g., Abrahamson *et al.*, 2008), and it underpins many building codes globally (e.g., Dobry *et al.*, 2000; Rey *et al.*, 2002).

Ideally, each seismic recording station would have some estimate of V_{S30} such that a GMPE could be calibrated appropriately. However, in Australia, this is the exception, rather than the norm. In recent years, Geoscience Australia has been investigating the use of various techniques from which to gather V_{S30} information at Australian seismic stations. This investigation has yielded the collection of 28 V_{S30} measurements at a variety of seismic stations across the continent located on a variety of rock types and ages (Collins *et al.*, 2006; Kayen and Carkin, 2006; Kayen *et al.*, 2010). The median V_{S30} of southeastern Australian sites classified as rock is approximately 830 m/s ($\pm$ 230 m/s). While the aforementioned value could be used to define the average shallow shear-wave velocity for an "average rock" site, it is unknown whether the current V_{S30} dataset is representative of average site conditions, or whether there may be a systematic bias associated with the selection of V_{S30} measurement sites.

In contrast, an estimate of κ_0 is known for all SEA stations with three or more records in the present dataset. Previous studies have shown that there are correlations between V_{S30} and κ_0. Consequently, a relationship between V_{S30} and κ_0 could potentially be obtained through correlating the two parameters for sites in Australia. The parameters are regressed using linear least squares with κ_0 being the independent variable so that a V_{S30} value can be obtained that correlates to the median κ_0 value of 0.006 sec (Fig 14). The correlation between V_{S30} and κ_0 can be described as:

$$V_{S30}(\kappa_0) = -7.42 \times 10^3 \, \kappa_0 + 864 \tag{17}$$

An R^2 value of 0.20 was obtained from the regression. Assuming the null hypothesis that there is no correlation between V_{S30} and κ_0, a *p*-value of 0.04985 was calculated. Using a significance level of 0.05 the null hypothesis cannot be accepted. However, it is noted from the R^2 value that the apparent correlation is very poor. Assuming the correlation holds, a V_{S30} of approximately 820 m/s is obtained assuming κ_0 of 0.006 sec. Consequently, the GMPE presented herein can be assumed to be appropriate for rock sites approximately near the B/C boundary in the NEHRP site classification scheme (Wills *et al.*, 2000; Building Seismic Safety Council, 2003).

Comparing the V_{S30} -κ_0 correlation above to other studies (Silva *et al.*, 1998; Chandler *et al.*, 2006; Van Houtte *et al.*, 2011), the corresponding value of average V_{S30} in the present study appears quite low relative to a κ_0 value of 0.006 sec. While it may be informative to compare these models with the current data, it should be recognised that the step-wise inversion of path and source parameters result in a unique suite of stochastic parameters that cannot be considered in isolation. While κ_0 is theoretically path independent, in the present analysis, this parameter is strongly tied to the anelastic attenuation function that has been applied. Consequently, it would be meaningless to compare the current V_{S30} -κ_0 correlation with the aforementioned studies because the path inversion process and subsequent data corrections are likely to influence the evaluation of κ_0.
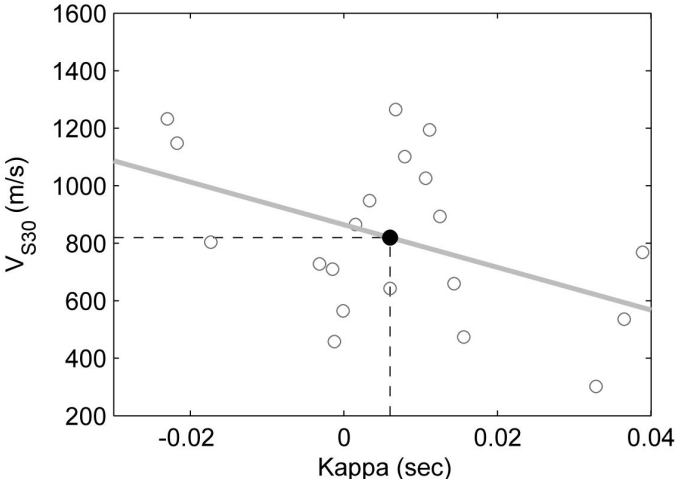
Figure 14: *The correlation between V_{S30} and κ_0 estimated at seismic stations in southeastern Australia. An R^2 value of 0.20 was obtained from the regression (grey line) indicating a very poor correlation between the two parameters. Assuming the correlation holds, a V_{S30} of approximately 820 m/s is obtained assuming $\kappa0$ of 0.006 sec (solid black circle).*

Regression of Model Coefficients

The stochastic simulations using the EXSIM model resulted in over 56,000 horizontal-component ground-motion simulations at 44 unique distances R_{rup}, logarithmically spaced from 1 to 422 km for earthquakes of magnitude $4.0 \leq M_W \leq 7.5$. These simulations were conducted for both the shallow and deep earthquake scenarios. Median response spectral accelerations were regressed using the Nelder-Mead minimization technique (The Mathworks, 2008) according to the functional form:

$$\log Y = c_0 + c_1 M_{ref} + c_2 M_{ref}^2 + \left(c_3 + c_4 M_{ref}\right) g_0 + \left(c_6 + c_7 M_{ref}\right) g_1$$
$$+ \left(c_9 + c_{10} M_{ref}\right) g_2$$

(18)

where Y is the 5% damped response pseudo spectral acceleration measured in cm/s^2 and:

$$M_{ref} = M_W - 4$$
$$r_1 = R_1 + c_8 M_{ref}$$
$$r_2 = R_2 + c_{11} M_{ref}$$
$$g_0 = \log\left(\sqrt{\min[R_{rup}, r_1]^2 + [1 + c_5 M_{ref}]^2}\right)$$
$$g_1 = \max[\log(R_{rup}/r_1), 0]$$
$$g_2 = \max[\log(R_{rup}/r_2), 0]$$

(19)

where R_{rup} is the closest distance to rupture in kilometres. The functional form chosen allows for variable geometrical attenuation with magnitude. It also comprises a variable geometrical hinge at different magnitudes (coefficients r_1 and r_2). This is because the assumption of a constant hinge across the magnitude range results in an unsatisfactory fit to the simulated data. Figure 15 shows the SEA rock response spectral acceleration simulations in each magnitude bin for the deep-earthquake model (i.e., high Brune stress drop) at a period of 1.0 second, regressed against the functional form above. The coefficient g_0 controls a magnitude-dependent rollover of response spectral accelerations at short rupture distances.

The regression coefficients for both the shallow- and deep-earthquake GMPEs are provided in Tables 7 and 8. Sample output data for validation of model application and unit testing purposes is provided in Appendix I.
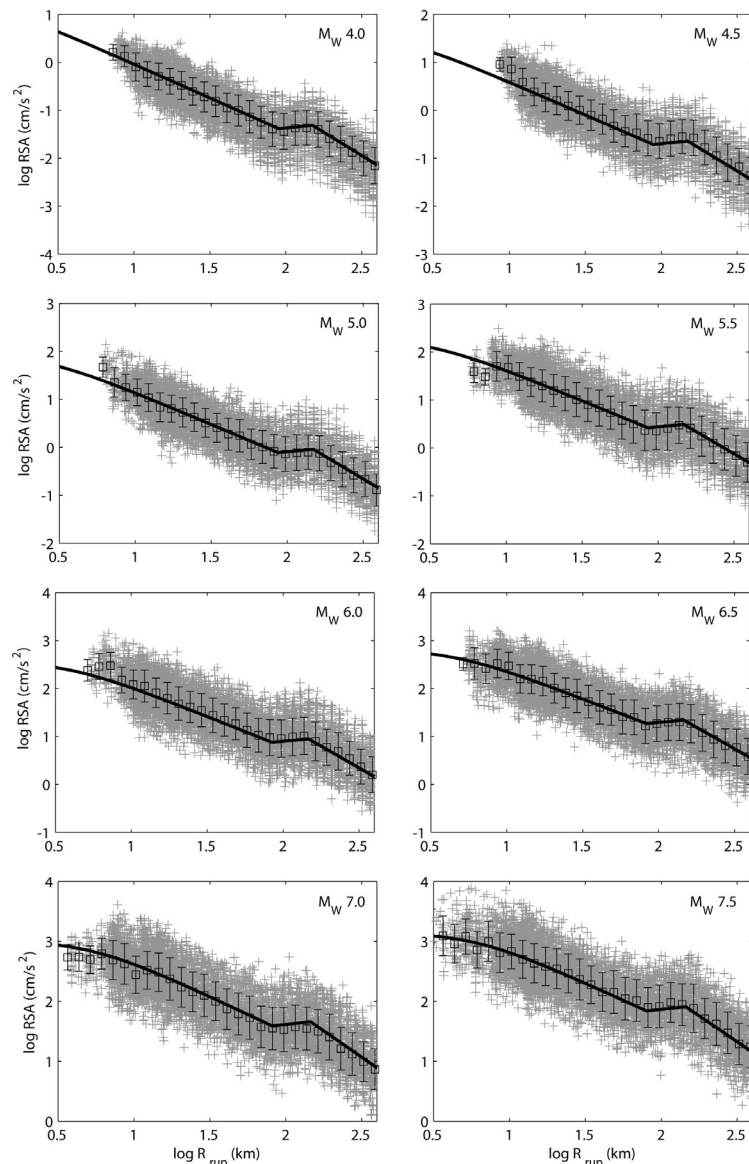
Figure 15: *Simulated 5% damped response spectral acceleration at a period of 1.0 s for the deep-earthquake model (i.e., high Brune stress drop). Each subplot shows the parametric form of Equations 18 and 19 (solid black lines) against the simulated data for each magnitude bin from M_W 4.0-7.5. The magnitude is indicated in the top-right corner of each subplot.*

Figure 16 shows the residuals of the simulated data against the regressed GMPE across a range of response spectral frequencies for M_W 6.5 earthquakes. This figure indicates that the chosen functional form has a very good correspondence to the simulated data. Finally, median response spectra are compared for the shallow- and deep-earthquake GMPEs for scenario earthquakes of M_W 5.0, 6.0, and 7.0 at a range of rupture distances (Figs. 17-19). Also shown in the series of Figures 17 through 19 is the Atkinson and Boore (1995) GMPE for ENA rock sites, Atkinson and Boore (2006) GMPE for ENA B/C crustal conditions, Chiou and Youngs (2008) for active California B/C crustal conditions, the Somerville et al. (2009) for non-cratonic Australia, and Pezeshk et al. (2011) for rock sites. These figures clearly demonstrate the influence of the Brune stress drop to the stochastic simulations with the deep-earthquake model resulting in larger short-period ground-motions than the shallow-earthquake model. At near-source rupture distances, the Atkinson and Boore (2006) GMPE behaves similarly to the SEA models at longer periods. This is most likely to be due to the use of a similar geometrical attenuation model at near-source distances.

The GMPEs developed in this study are observed to predict higher near-source ground motions relative to the Somerville *et al.*(2009) non-cratonic GMPE, particularly shorter periods (Figs. 20-21). However, because of the use of higher geometrical attenuation rates from the new SEA GMPEs, there is a transition to higher ground motions at most periods between approximately 20-50 km using Somerville *et al.*(2009). At a rupture distance of 200 km, the Atkinson and Boore (2006) GMPE long-period ground motions are similar to those of the GMPEs developed herein. However, at distances beyond 200km, the differences between long-period ground motions become more obvious and the Atkinson and Boore (2006) GMPE estimates higher response spectra across all periods of shaking because of the assumption of lower geometrical attenuation at larger distances (Figs. 20-21). This trend is consistent with empirical observations of average ground-motion attenuation observed between the ENA and SEA stable continental regions (Allen and Atkinson, 2007).

The GMPEs developed herein are also broadly consistent with the Chiou and Youngs (2008) GMPE developed for California as part of the Next Generation Attenuation (NGA) Project (Power *et al.*, 2008), particularly for magnitudes approximately $M_W \geq 6.0$ at distances less than 100 km. This indicates that the magnitude scaling of the stochastic models developed herein are consistent with the purely empirical models of Chiou and Youngs (2008). At smaller magnitudes, however, the Chiou and Youngs (2008) empirical GMPE estimates larger long-period response spectral acceleration than the southeastern Australian stochastic models. It is now well acknowledged by the global ground-motion modeling community that the GMPEs developed as part of the NGA Project consistently overestimate ground-motions for earthquakes of approximately M_W 5.5 and less (e.g., Atkinson and Morrison, 2009; Chiou *et al.*, 2010; Atkinson and Boore, 2011; Campbell, 2011). Consequently, the differences observed between the new southeastern Australian and California models in Figure 17 may simply be an artifact of the empirical modeling process and data used by the NGA group modelers. More research is required to determine whether differences, or similarities, between active tectonic and stable continent data are statistically significant
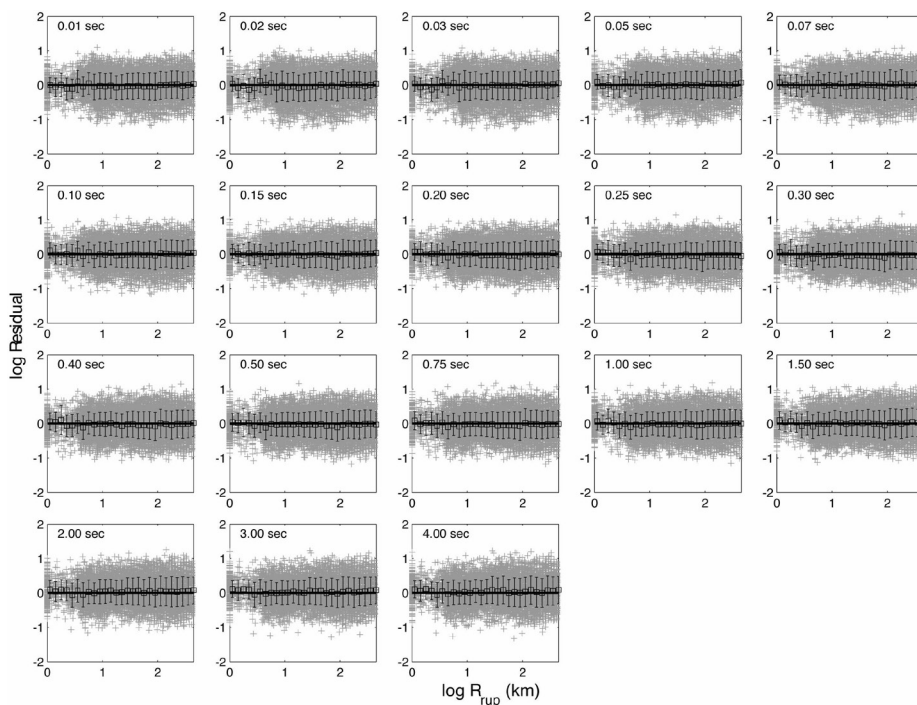
Figure 16: *Residuals (in units of log Y), defined as the simulated data minus the regressed GMPE, for the shallow, low-stress drop model (Table 7), across a range of response spectral frequencies for M_W 6.5 earthquakes. Grey crosses indicate individual residuals, which are logarithmically binned in 0.1 log-km windows. Black squares indicate mean and standard deviations for each distance window.*

Table 7: Coefficients for predicting 5% damped PSA for median horizontal component ground motions for shallow (h < 10 km) earthquakes for average SEA site conditions. Response spectral values Y are given as $\log_{10}$ cm/s^2 according to the functional form given in Equations 18 and 19.

PERIOD (SEC)	c_0	c_1	c_2	c_3	c_4	c_5	c_6	c_7	c_8	c_9	c_{10}	c_{11}	σ
0.01	3.259	0.505	-0.069	-1.839	0.158	1.247	-0.204	-0.044	-5.100	-2.862	0.251	-0.639	0.412
0.02	3.368	0.496	-0.062	-1.808	0.136	1.247	-0.486	0.017	-4.677	-2.865	0.244	-0.776	0.438
0.03	3.511	0.471	-0.060	-1.852	0.142	1.434	-0.545	0.015	-4.983	-2.849	0.250	-1.103	0.431
0.05	3.545	0.477	-0.063	-1.837	0.140	1.459	-0.489	-0.011	-5.109	-3.073	0.301	-1.178	0.399
0.08	3.516	0.492	-0.068	-1.806	0.142	1.418	-0.341	-0.043	-4.994	-3.251	0.309	-0.904	0.381
0.10	3.458	0.515	-0.073	-1.774	0.142	1.375	-0.216	-0.061	-4.849	-3.284	0.274	-0.467	0.372
0.15	3.296	0.580	-0.082	-1.700	0.131	1.286	-0.062	-0.067	-4.641	-3.123	0.158	0.538	0.364
0.20	3.136	0.642	-0.092	-1.648	0.127	1.214	0.072	-0.080	-4.663	-2.936	0.106	1.089	0.359
0.25	2.998	0.692	-0.101	-1.615	0.130	1.159	0.207	-0.105	-4.828	-2.789	0.112	1.256	0.358
0.30	2.872	0.736	-0.110	-1.593	0.135	1.121	0.317	-0.126	-4.911	-2.678	0.132	1.193	0.356
0.40	2.623	0.818	-0.124	-1.565	0.140	1.082	0.432	-0.128	-4.484	-2.539	0.137	0.621	0.354
0.50	2.398	0.889	-0.134	-1.548	0.140	1.070	0.468	-0.104	-3.733	-2.461	0.114	-0.111	0.352
0.75	1.944	1.011	-0.147	-1.527	0.140	1.050	0.481	-0.088	-3.243	-2.413	0.121	-1.055	0.350
1.00	1.616	1.078	-0.151	-1.522	0.145	1.025	0.484	-0.121	-3.942	-2.442	0.187	-1.130	0.349
1.50	1.193	1.102	-0.142	-1.540	0.160	1.009	0.504	-0.159	-4.242	-2.499	0.256	-0.703	0.349
2.00	0.929	1.074	-0.126	-1.564	0.175	1.016	0.522	-0.164	-3.762	-2.526	0.267	-0.293	0.348
3.00	0.574	1.011	-0.095	-1.588	0.185	1.048	0.514	-0.158	-3.784	-2.536	0.268	-0.054	0.347
4.00	0.340	0.954	-0.071	-1.604	0.189	1.071	0.509	-0.158	-4.199	-2.565	0.286	-0.108	0.346

Table 8: *Coefficients for predicting 5% damped PSA for median horizontal component ground motions for deep (h $\geq$ 10 km) earthquakes for average SEA site conditions. Response spectral values Y are given as $\log_{10}$ cm/s^2 according to the functional form given in Equations 18 and 19.*

PERIOD (SEC)	c_0	c_1	c_2	c_3	c_4	c_5	c_6	c_7	c_8	c_9	c_{10}	c_{11}	σ
0.01	3.383	0.604	-0.091	-1.929	0.175	1.429	-0.182	-0.013	-4.699	-3.149	0.316	-0.765	0.365
0.02	3.557	0.590	-0.086	-1.940	0.162	2.186	-0.455	0.034	-4.863	-3.093	0.305	-1.284	0.390
0.03	3.707	0.528	-0.084	-1.973	0.186	0.967	-0.455	0.002	-4.683	-3.285	0.393	-1.260	0.384
0.05	3.739	0.546	-0.084	-1.937	0.165	1.740	-0.440	0.001	-4.337	-3.478	0.418	-1.128	0.356
0.08	3.672	0.584	-0.089	-1.888	0.158	0.656	-0.299	-0.033	-4.186	-3.553	0.398	-1.194	0.339
0.10	3.579	0.627	-0.097	-1.848	0.157	-0.122	-0.164	-0.058	-4.049	-3.517	0.345	-1.087	0.332
0.15	3.378	0.728	-0.113	-1.780	0.148	1.127	-0.009	-0.045	-3.626	-3.284	0.185	-0.325	0.327
0.20	3.183	0.821	-0.128	-1.733	0.144	2.006	0.123	-0.043	-3.487	-3.059	0.108	-0.016	0.325
0.25	3.004	0.899	-0.143	-1.701	0.148	1.902	0.260	-0.063	-3.599	-2.884	0.106	-0.177	0.325
0.30	2.843	0.963	-0.156	-1.679	0.154	1.532	0.369	-0.084	-3.751	-2.750	0.124	-0.478	0.325
0.40	2.550	1.065	-0.172	-1.652	0.159	1.227	0.461	-0.095	-3.856	-2.560	0.130	-0.996	0.325
0.50	2.303	1.139	-0.181	-1.637	0.160	1.367	0.462	-0.083	-3.790	-2.437	0.109	-1.334	0.323
0.75	1.822	1.248	-0.186	-1.615	0.158	1.708	0.453	-0.077	-3.632	-2.381	0.117	-1.557	0.319
1.00	1.479	1.297	-0.182	-1.603	0.157	1.706	0.487	-0.101	-3.612	-2.471	0.182	-1.411	0.318
1.50	1.071	1.274	-0.161	-1.626	0.173	1.651	0.526	-0.135	-3.723	-2.564	0.248	-0.982	0.316
2.00	0.841	1.206	-0.139	-1.664	0.194	1.660	0.539	-0.148	-3.764	-2.581	0.261	-0.654	0.314
3.00	0.534	1.096	-0.105	-1.707	0.218	1.616	0.598	-0.167	-3.160	-2.707	0.309	-0.405	0.311
4.00	0.284	1.098	-0.108	-1.713	0.215	1.381	0.569	-0.182	-4.105	-2.797	0.367	0.177	0.345
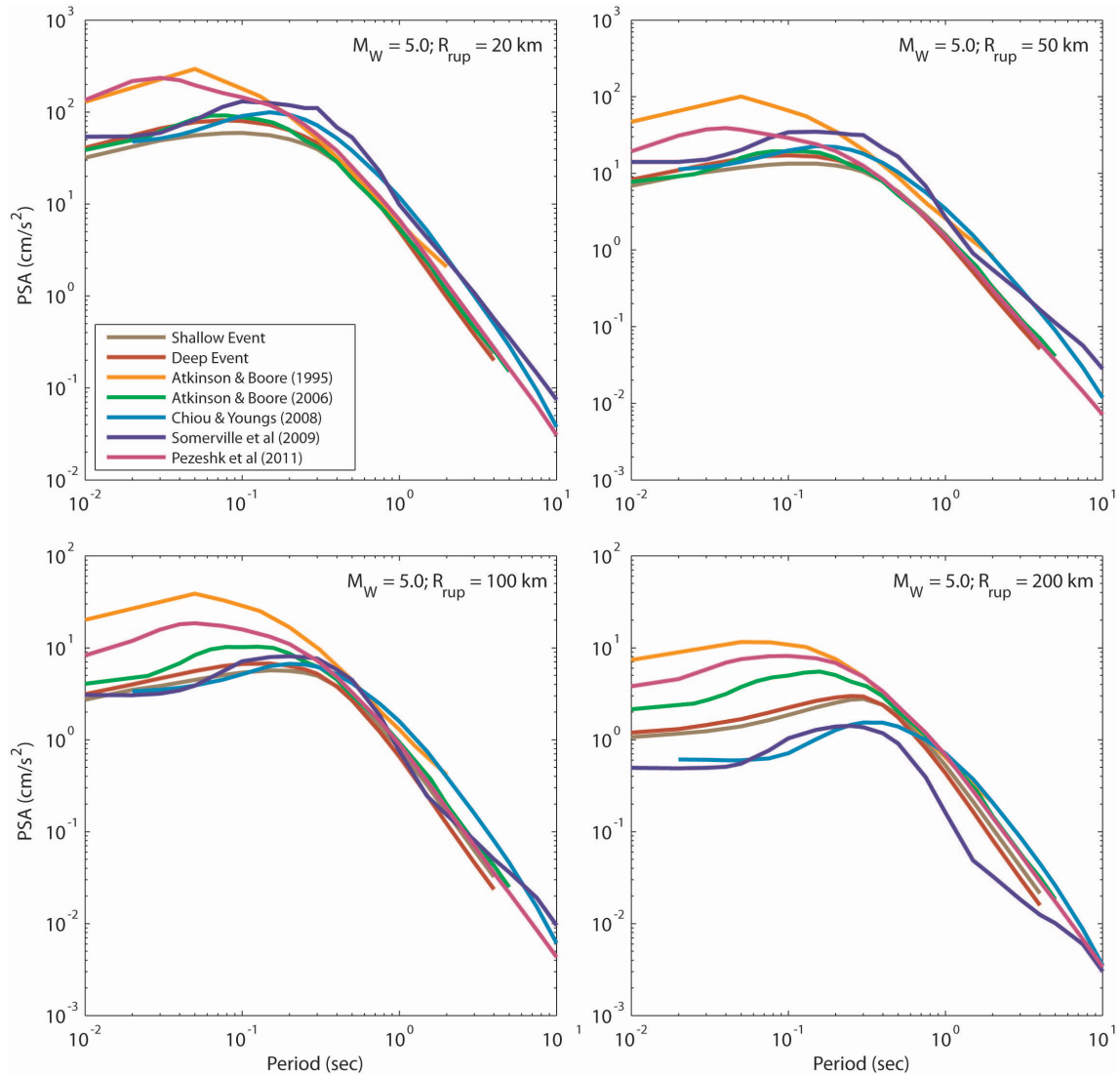
Figure 17: *Comparison of the median 5% damped response spectral acceleration response spectra for the shallow- and deep-earthquake GMPEs for a scenario M_W 5.0 earthquake at a range of rupture distances. Also indicated for comparison is the Atkinson and Boore (1995) GMPE for ENA rock sites ($V_{S30} \geq 2,800$ m/s), Atkinson and Boore (2006) GMPE for ENA B/C crustal conditions, Chiou and Youngs (2008) for California crustal B/C conditions, the Somerville et al. (2009) for non-cratonic Australia ($V_{S30} = 865$ m/s), and Pezeshk et al. (2011) for rock sites ($V_{S30} \geq 2,000$ m/s).*
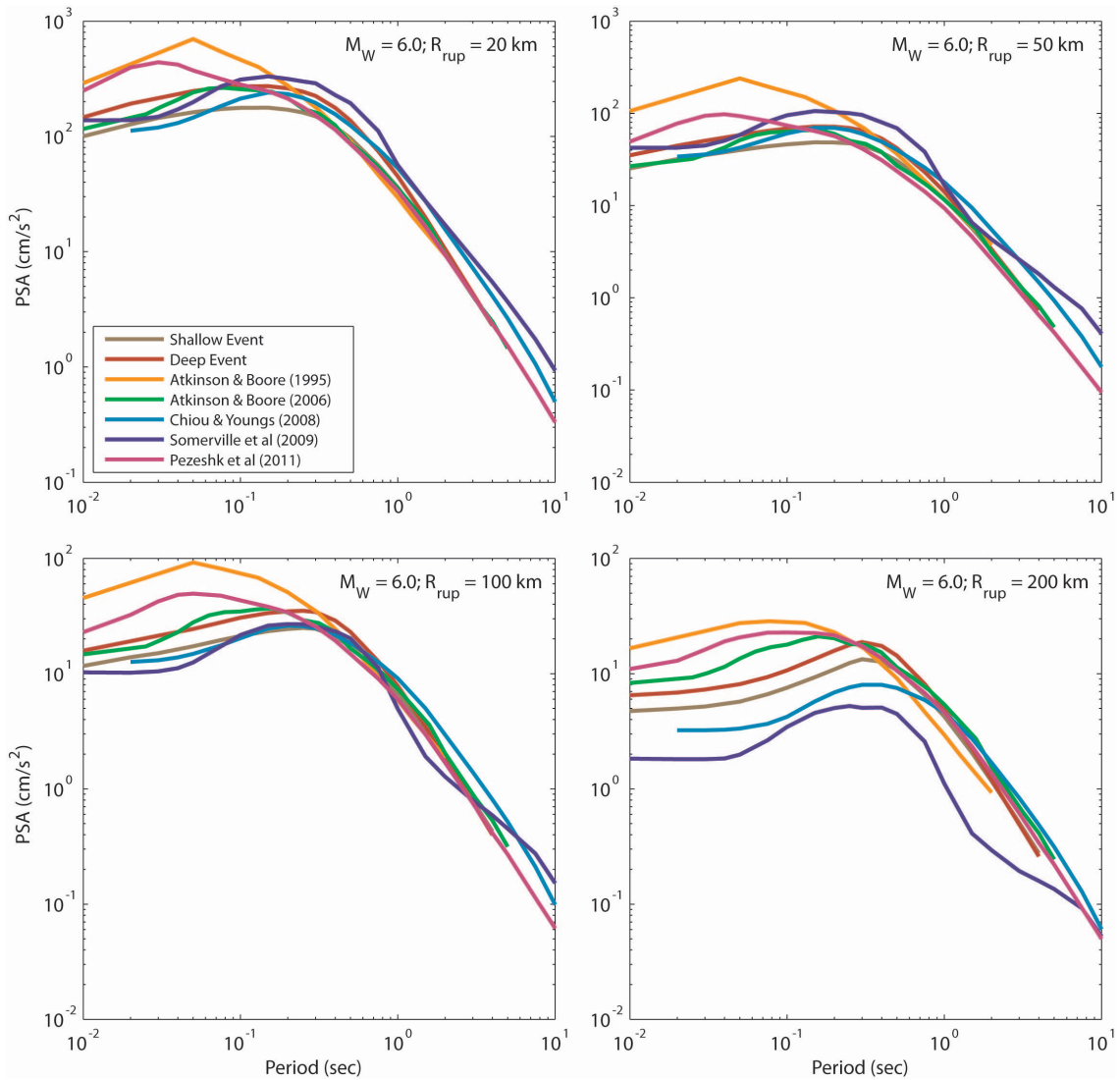
Figure 18: *Comparison of the median 5% damped response spectral acceleration response spectra for the shallow- and deep-earthquake GMPEs for a scenario M_W 6.0 earthquake at a range of rupture distances. Also indicated for comparison is the Atkinson and Boore (1995) GMPE for ENA rock sites ($V_{S30} \geq 2,800$ m/s), Atkinson and Boore (2006) GMPE for ENA B/C crustal conditions, Chiou and Youngs (2008) for California crustal B/C conditions, the Somerville et al. (2009) for non-cratonic Australia ($V_{S30} = 865$ m/s), and Pezeshk et al. (2011) for rock sites ($V_{S30} \geq 2,000$ m/s).*
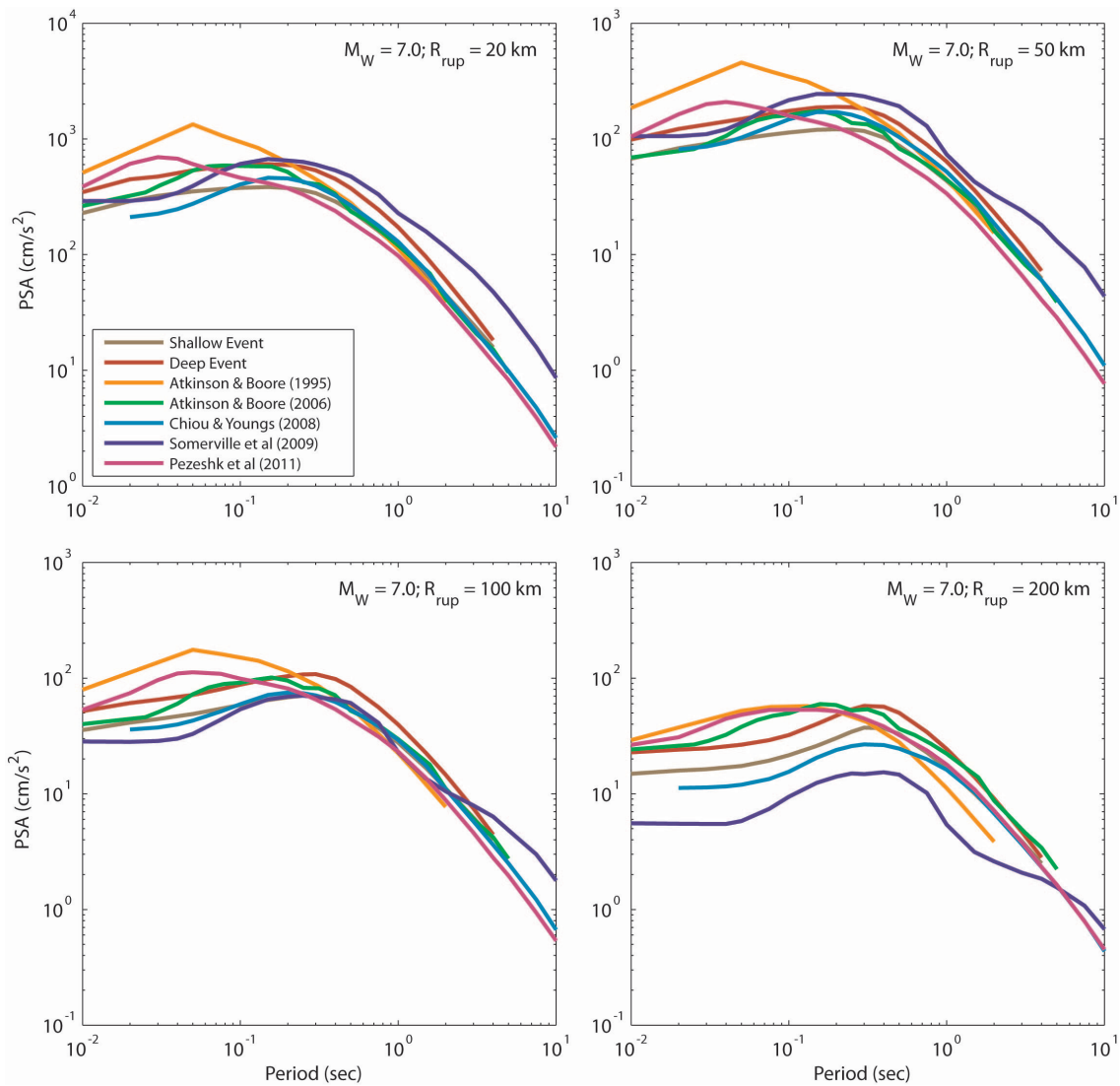
Figure 19: *Comparison of the median 5% damped response spectral acceleration response spectra for the shallow- and deep-earthquake GMPEs for a scenario M_W 7.0 earthquake at a range of rupture distances. Also indicated for comparison is the Atkinson and Boore (1995) GMPE for ENA rock sites ($V_{S30} \geq 2,800$ m/s), Atkinson and Boore (2006) GMPE for ENA B/C crustal conditions, Chiou and Youngs (2008) for California crustal B/C conditions, the Somerville et al. (2009) for non-cratonic Australia ($V_{S30} = 865$ m/s), and Pezeshk et al. (2011) for rock sites ($V_{S30} \geq 2,000$ m/s).*
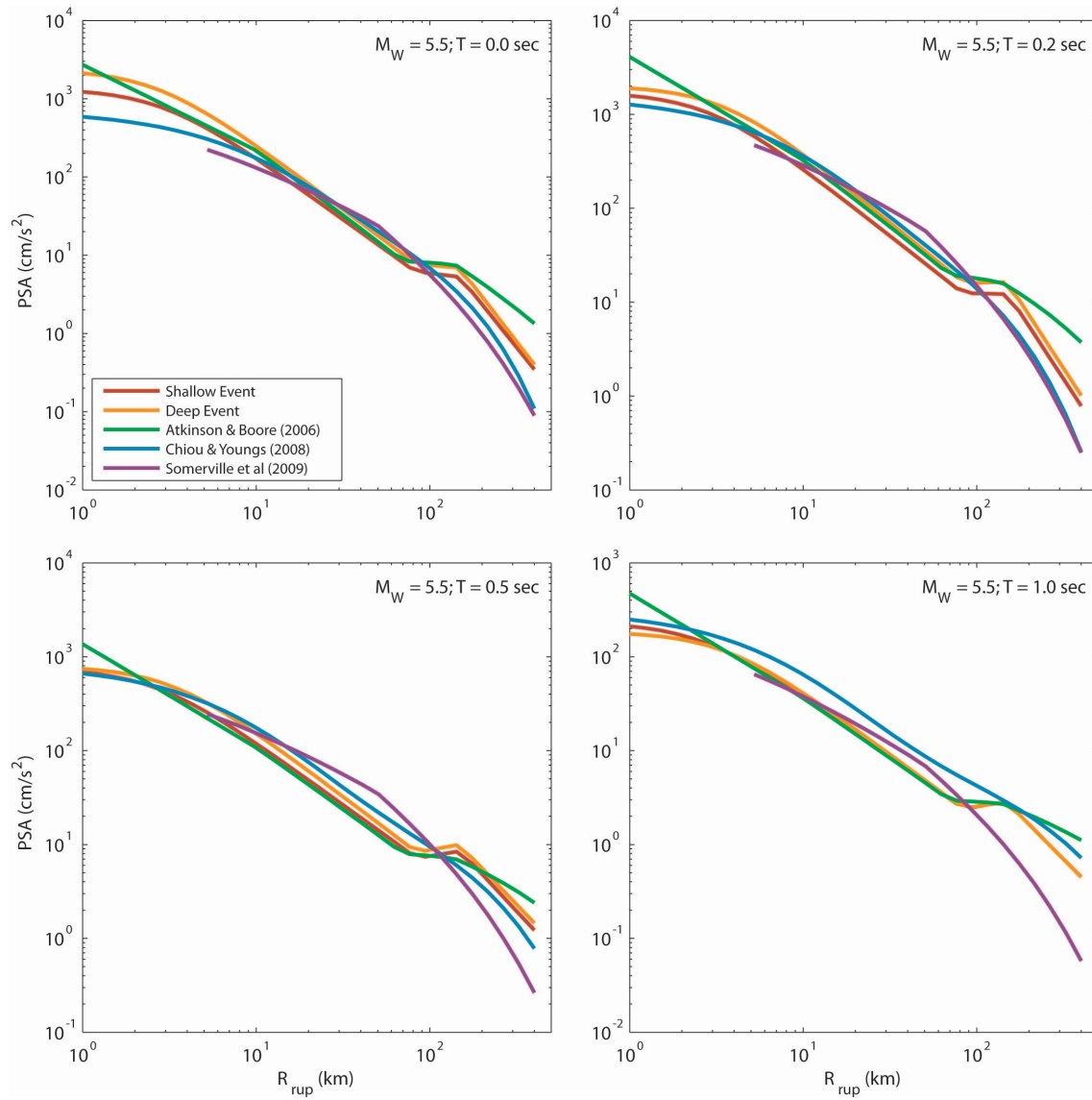
Figure 20: *Comparison of the median horizontal 5% damped response spectral acceleration response spectra for the shallow- and deep-earthquake GMPEs for a scenario M_W 5.5 earthquake against R_{rup} for a series of response spectral periods, T. Also indicated for comparison is the Atkinson and Boore (2006) GMPE for ENA B/C crustal conditions, Chiou and Youngs (2008) for active crustal California and the Somerville et al. (2009) for non-cratonic Australia. The R_{rup} distance metric is converted to Joyner-Boore distance RJB for use in the Somerville et al. (2009) GMPE. In this case, the scenario earthquake is treated as a point source with a hypocentral depth of 5 km. Consequently the minimum corresponding R_{rup} value applicable in the Somerville et al. (2009) GMPE is 5 km.*
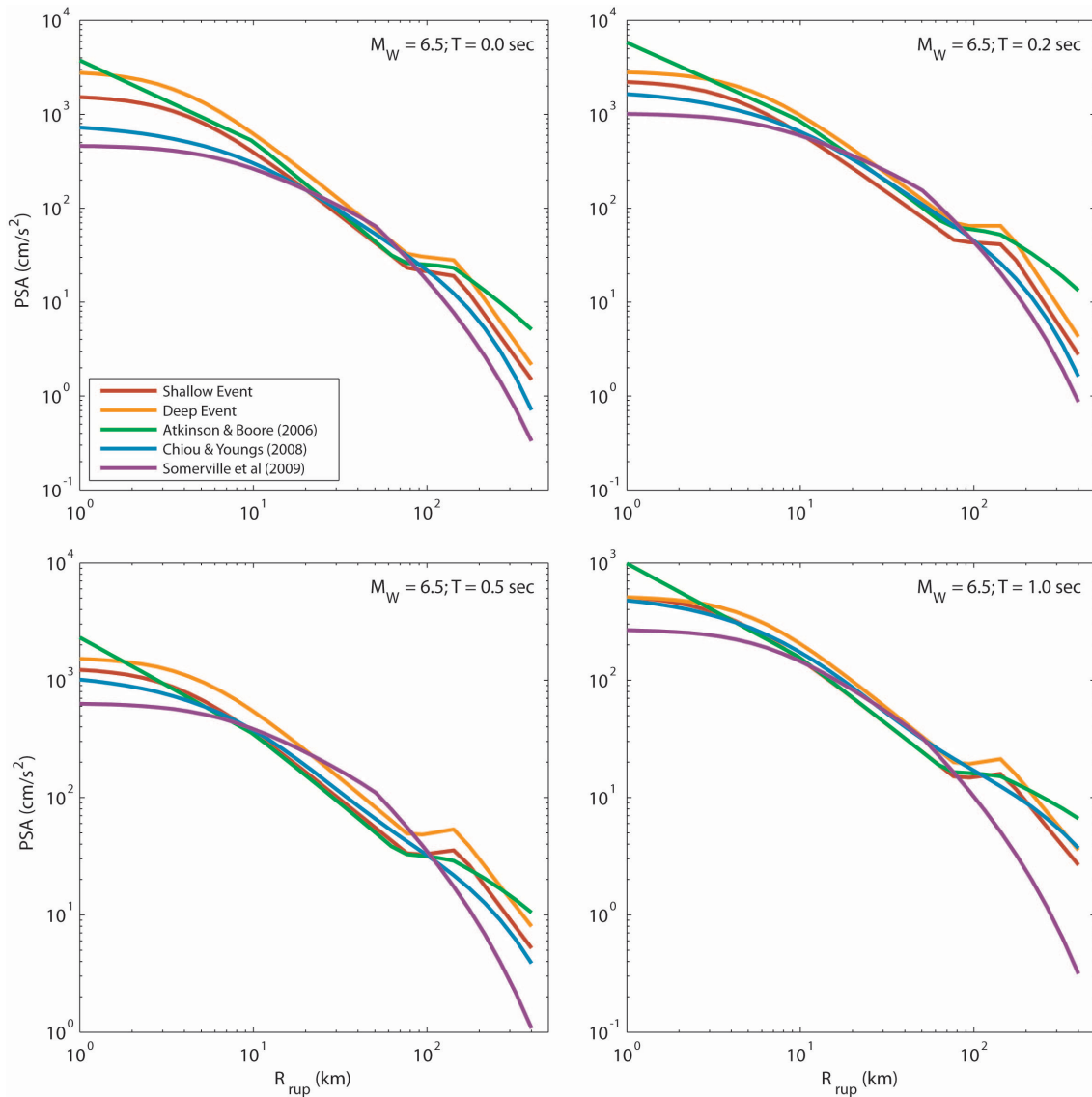
Figure 21: *Comparison of the median horizontal 5% damped response spectral acceleration response spectra for the shallow- and deep-earthquake GMPEs for a scenario M_W 6.5 earthquake against R_{rup} for a series of response spectral periods, T. Also indicated for comparison is the Atkinson and Boore (2006) GMPE for ENA B/C crustal conditions, Chiou and Youngs (2008) for active crustal California and the Somerville et al. (2009) for non-cratonic Australia. This scenario assumes a vertically dipping fault, which cases surface rupture. In this case, $R_{rup} = R_{JB}$.*

Comparison of GMPEs against Recorded Data

COMPARISON AGAINST RECORDED EASTERN AUSTRALIAN DATA

It is useful to compare the new GMPEs for SEA against recorded ground-motion data from the region to review their applicability for use in hazard studies. Unfortunately, we do not possess any recorded ground-motions from large-magnitude earthquakes in SEA – as is the case in many stable continental regions. However, the limited moderate-magnitude data that are available can be used to validate the stochastic ground-motion models. Five percent damped response spectral accelerations are calculated for time histories from all earthquakes of $M_W \geq 4.0$ compiled for the empirical Fourier analysis above. The geometric mean of the two horizontal components for each record was then calculated. The median ground-motion residuals were calculated for near-source data ($R_{rup} \leq 80$ km) and moderate-to-large distances ($R_{rup} > 80$ km) for response spectra between periods of 0.04-4.0 s (Fig. 22). The results indicate generally low residuals across the full range of spectral periods within the range of the model uncertainty.
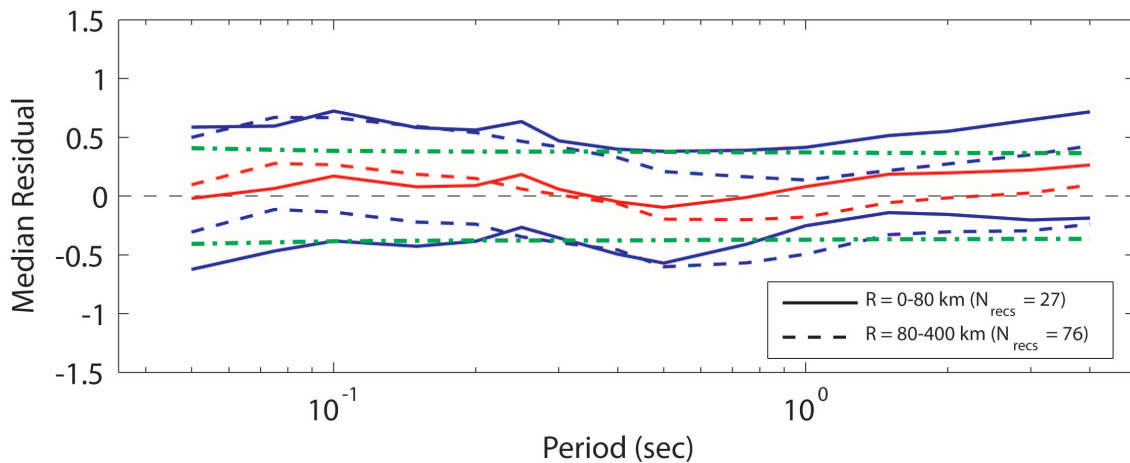
Figure 22: *Residuals (log10 observed – log10 predicted) of 5% damped response spectral accelerations recorded from all $M_W \geq 4.0$ earthquakes in southeastern Australia at distances R_{rup} less than 80 km (solid lines) and 80-300 km (dashed lines), respectively. Median residuals (red lines) are plotted against spectral period with ± 1σ indicated (blue lines). The model sigma (Table 7) for the shallow-earthquake model is also plotted (green dot-dashed lines) relative to the zero residual line (thin black dashed line).*

In evaluating the performance of any model, it is prudent to test the model with an independent dataset that was not used in the derivation of the model itself. Owing to the limited dataset with which the empirical relations were developed above, there are very few Australian data available to undertake such rigorous analyses. However, as discussed above, the attenuation parameters (i.e., geometrical and anelastic attenuation) were developed only using data from earthquakes with three or more recordings within 100 km from the earthquake source. As a consequence, some of the $M_W \geq 4.0$ data were not directly used for the derivation of the attenuation parameters (see Table 2). While some of these data have been included in the derivation of median source parameters (e.g., Brune stress drop), it is considered that these data can be used as a relatively independent dataset to validate the proposed GMPEs. Only three events could be used for this exercise: the 1) 1994 Ellalong, NSW; 2) 2001 Swan Hill, VIC, and; 3) 2011 Bowen, QLD earthquakes. Unfortunately, none of these events had a recording on a rock site at a rupture distance R_{rup} less than 80 km. Consequently, the validation of the GMPE for the short distance could not be considered (Fig. 23). However, the use of data not employed for the inversion of the geometrical and anelastic attenuation parameters at distances between 80 and 400 km, results in relatively small residuals with respect to the proposed model (Fig. 23). While there are small biases associated with this comparison, the GMPE generally performs well against the proposed independent dataset with the median residuals for the larger rupture distances within the uncertainty bounds of the GMPE developed herein.
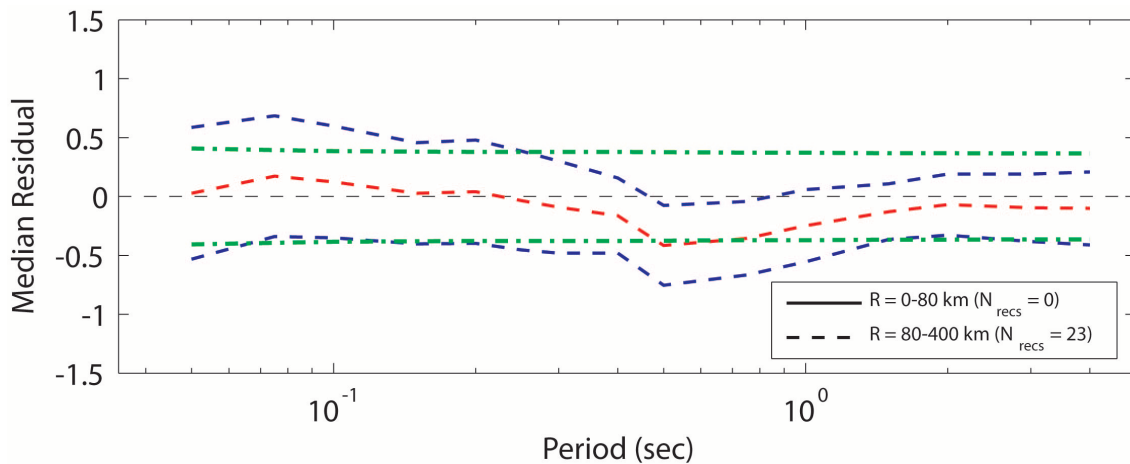
Figure 23: *Residuals (log10 observed – log10 predicted) of 5% damped response spectral accelerations recorded from earthquakes $M_W \geq 4.0$ in southeastern Australia not used to determine attenuation parameters (i.e., those events in Table 2 without an asterisk (*) in the final column). See Figure 22 caption for detailed description of figure contents.*

COMPARISON AGAINST RECORDED WESTERN AUSTRALIAN DATA

Finally, the new GMPEs are used to assess their applicability outside of the SEA region. Allen *et al*. (2006) compiled a dataset of strong- and weak-motion data from an earthquake sequence in the Archean-aged Yilgarn Craton of Western Australia (WA). In this sequence, seven earthquakes of magnitudes between M_W 4.0-4.6 were recorded. While Allen *et al*. (2006) urge some caution in the use of these data owing to the swarm-like nature of the events and the limited spatial distribution of the recordings (both in distance and azimuth), the dataset can still be treated as an independent test of the GMPEs proposed herein. Performing the same analysis for the WA data, again low median residuals are observed, particularly at short rupture distances (Fig. 24). The model slightly underestimates longer period response spectra. This is because almost all of the records from the WA dataset were recorded at hypocentral depths less than 2.5 km (Allen *et al*., 2006). Consequently, many of the records possess a strong *Rg*-phase which dominate the spectra for some of the records and this effect is not considered in the current model for SEA. Nevertheless, the positive result was unexpected because of several prior studies suggesting lower attenuation in the WA region (Gaull *et al*., 1990; Leonard *et al*., 2007). However, the distance range of the WA data was limited to stations less than 200 km from the earthquake sources. Accordingly, differences in attenuation between regions may not be perceptible in this limited distance range. Moreover, as an analogy to the attenuation of response spectra, there are only relatively minor differences between local magnitude M_L formulae at distances less than 200 km between eastern and western Australia (Allen, 2010). These distances are most relevant in PSHA, where the hazard is dominated generally by near-source ground motions. This supports the current observation that near-source response spectral accelerations can be approximated using GMPEs derived for eastern Australian earthquakes, particularly at short periods.
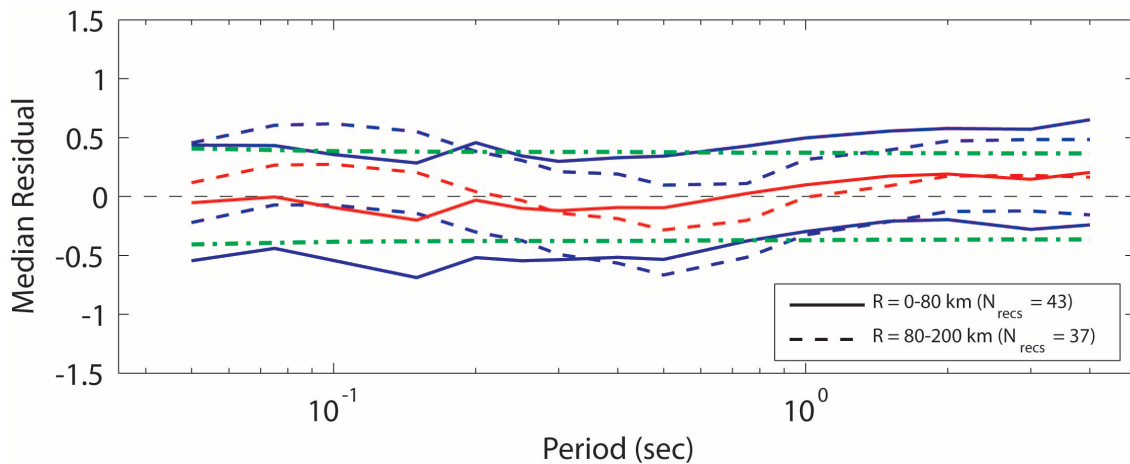
Figure 24: *Residuals (log10 observed – log10 predicted) of 5% damped response spectral accelerations recorded from earthquakes $M_W \geq 4.0$ in Western Australia relative to the southeastern Australian model. See Figure 20 caption for detailed description of figure content.*

COMPARISON AGAINST THE 19 JUNE 2012, M_W 5.0 MOE, VICTORIA EARTHQUAKE

As this manuscript was being finalised, a M_W 5.0 earthquake occurred near the township of Moe, southeastern Victoria. The earthquake was widely felt across the state and caused minor damage to residential and commercial structures (Civil Engineers Australia, 2012). The earthquake, which occurred in the Victoria's primary electricity generation region also temporarily disabled three of the four units at nearby the Loy Yang A power station, Victoria's largest coal-fired power station. This earthquake was well recorded by seismic stations operated by Environmental Systems and Services, as well as by Geoscience Australia's National Seismic Network, with at least eight stations within about 100 km of the earthquake's epicentre. At the time of writing, only data from two of these stations have been compiled by the author; the first from Jeeralang Junction (JENM) at approximately R = 26 km to the southeast of the epicentre; and the second from Toolangi (TOO) at approximately R = 97 km to the northwest of the epicentre. Given the hypocentral depth of 11 km for this earthquake, the deep-earthquake GMPE for southeastern Australia was compared to data from the two aforementioned stations (Fig. 25). Overall, the model shows an excellent fit to the recorded data for both stations.
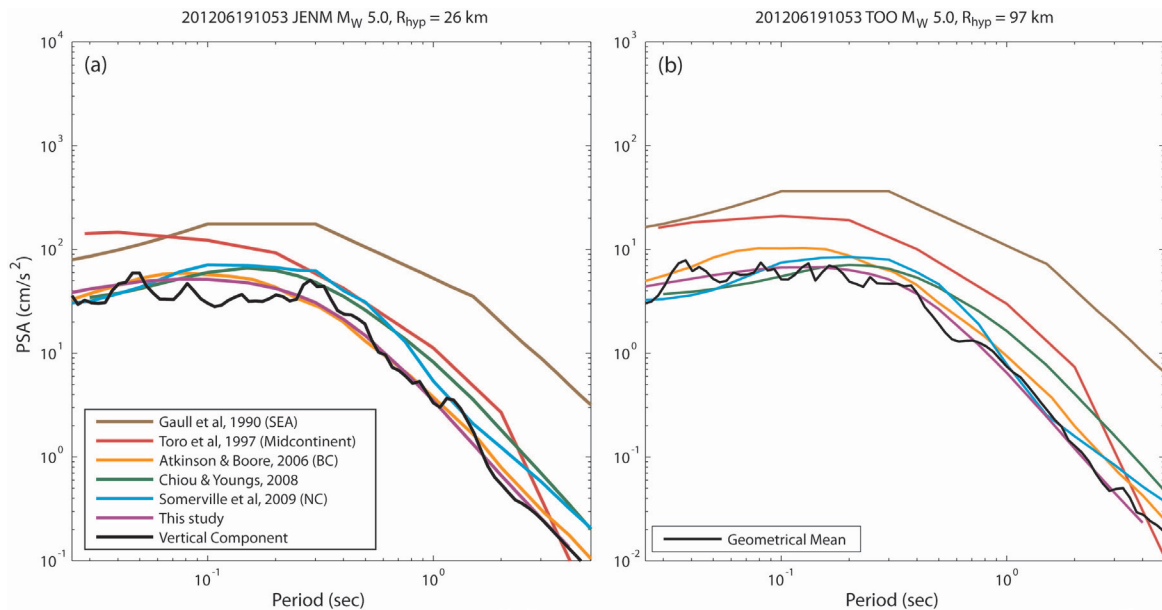
Figure 25: *Comparison of the median 5% damped response spectral acceleration from the 19 June 2012 M_W 5.0 earthquake near Moe, Victoria, recorded on seismographs located at (a) Jeeralang Junction (JENM) and (b) Toolangi (TOO). The JENM record is from a vertical-component short-period velocity sensor and a sample rate of 100 Hz, while the record from TOO is the geometrical mean of the two horizontal components recorded on a broadband seismometer and a sample rate of 200 Hz. The recorded data are compared to several modern GMPEs, including the model presented herein. Due to the earthquake's hypocentral depth of 11 km, the deep focus model is used for comparison here. The Gaull et al. (1990) PGA attenuation model is tied to the AS1170.4 spectral shape factors for rock sites (Standards Australia, 2007). In general, the southeastern Australian GMPE developed herein provides an excellent fit to the observed data from the 2012 Moe earthquake.*

Discussion

The current study uses the stochastic methodology described in Boore (1993; 2003) to develop a GMPE suitable for use for earthquake hazard assessments in southeastern Australia. While this study represents a step forward in Australian ground-motion modelling, it is important to recognise that there are still important limitations of the models produced herein and the stochastic ground-motion simulation software used. As discussed above, it has been recognised by Atkinson *et al.* (2009) that finite-fault ground-motion simulations for small earthquakes (approximately M_W 5.0) using EXSIM do not compare well with point source simulations (e.g., Boore, 2003) at large distances ($R \geq 100$ km), where it should be expected that the two simulation techniques would agree. It was observed by Boore (2009) that these differences could be minimised by using fewer subfaults in the ground-motion simulations in EXSIM. Boore (2009) subsequently modified the EXSIM source code such that the simulated ground motions at large distances were more consistent with point-source simulations from the SMSIM package. However, the updated EXSIM package was not configured for GMPE development and could not be used in this study. The Motazedian and Atkinson (2005) implementation of EXSIM as used in Atkinson and Boore (2006) was extensively modified for the purpose of randomising the input stochastic parameters for GMPE development. In the current study, the number of subfaults was set to three for all simulations in an attempt to minimise the limitations in using the Motazedian and Atkinson (2005) implementation of EXSIM. It is recognised that the GMPEs presented herein should be updated using the latest version of EXSIM, correctly configured to generate stochastic datasets that can be used to develop GMPEs. This work is planned and will commence following discussions with Gail Atkinson and David Boore later in 2012. Despite this limitation, it is observed from the analysis above that these models can still be considered appropriate for southeastern Australian crustal conditions and they result in small residuals when compared to observed data across all response spectral periods. In contrast, many of the other GMPEs that were developed for Australia and other stable continental regions considered for use in the Australian National Earthquake Hazard Map do not appear to be consistent with observed ground-motions (Allen *et al.*, 2011; Burbidge, 2012).

The Brune stress drops calculated herein are based on the correction of recorded Fourier displacement spectra using geometrical spreading models, anelastic attenuation factors and path-independent kappa estimates. One potentially important factor that was not considered in the inversion of stress drop is the effect of crustal amplification factors on the correction to an average source spectrum for each earthquake considered. In the present study, vertical-component records are used in the inversion of all source and attenuation parameters under the assumption that they are unaffected by crustal amplification effects. Rather, the H/V ratio is used as a crude approximation of the near-surface amplification for rock sites on horizontal components (Chen and Atkinson, 2002; Atkinson, 2004). If this assumption is erroneous and vertical-component ground-motions are affected by crustal amplifications, this will affect the inversion of the Brune source spectrum, particularly at higher frequencies. The net effect of not considering potential crustal amplifications, if they are significant, is that it may yield estimates Brune stress drop that are too high. This issue will be the focus of further investigations.

Users of the GMPEs presented in the current study will note relatively large values of ground-motion uncertainty σ. The values presented in Tables 7 and 8 are approximately 0.41 to 0.36 (log base 10 units) for short periods for the shallow and deep GMPEs, respectively. In contrast to our values, Atkinson and Boore (2006) recommend $\sigma = 0.30$, while Somerville *et al.* (2009) recommend $\sigma = 0.24$. The reason for the apparent large values in ground-motion uncertainty is partially due to the aleatory uncertainty of input parameters assigned in the stochastic simulations. In particular, the relatively large uncertainty on the assumed κ_0 values is a major contributor at high frequencies. This study assumes normally distributed variability of path independent κ_0 with a median of 0.006 ± 0.017 s based on observations from recoded data. In contrast Atkinson and Boore (2006) used a uniform distribution between 0.002 and 0.008 s for their simulations. Based on the distribution of kappa values for sites in eastern Australia (Fig. 9), a smaller distribution cannot be justified at this time. With further research, the uncertainty associated with the stochastic input parameters for eastern Australian earthquakes should be reduced.

Another limitation of the GMPEs presented herein is that they are presently only calibrated to average rock conditions in southeastern Australia. Based on the limited V_{S30} measurements obtained in Australia, and κ_0 values determined in the present study, the present GMPEs are appropriate for a V_{S30} site condition of approximately 820 m/s. The requirements for the Australian earthquake loading code AS1170.4 (Standards Australia, 2007) require earthquake hazard to be estimated on a reference B/C boundary rock site. Based on the NEHRP site classification scheme, the average V_{S30} of approximately 820 m/s to which the GMPEs were calibrated can be considered as B/C reference rock (Building Seismic Safety Council, 2003). As a consequence the models are approximately consistent with the requirements of the Australian Standards and should not require any further adjustments for use in the national hazard map (Burbidge *et al.*, 2010; Burbidge and Leonard, 2011).

Because most seismic recording stations in Australia are located on rock sites, there are very few data from which to determine empirically-based site amplification factors for different seismic site conditions. Consequently, it will be necessary to develop scaling factors from either simulated data, or by adopting site amplification factors from other studies (e.g., Choi and Stewart, 2005). As discussed above, the requirements for the Australian Standard AS1170.4 (Standards Australia, 2007) require earthquake hazard to be estimated on a B/C boundary reference site, with site-specific amplification coefficients for design spectra being considered in the building code provisions. Therefore, there is no requirement to develop these amplification factors for use in the national hazard model. However, to make these GMPEs more broadly applicable, it is desirable to incorporate this functionality into the parametric form of the models. This will be the focus of future work.

Because there are very few ground-motion records for large earthquakes in stable continental regions, one of the key uncertainties is how ground-motions scale from moderate-to-large magnitude earthquakes. Recently, some studies have suggested similarities between active crustal and stable continental ground motions for small-to-moderate magnitude earthquakes at near sources and low frequencies (Atkinson and Morrison, 2009). If it can be shown that the similarities at small magnitudes persist to larger events, then active tectonic GMPEs may be useful to guide the development of GMPEs for use in stable continental regions. This may also negate the need to develop purely stochastic GMPEs as developed herein. In contrast, we may simply rely on active tectonic data to define the near-source long-period scaling, with adjustments for short-period and long-distance effects, such as those adjustments used in GMPEs developed using the Hybrid Empirical Method (e.g., Campbell, 2003; Pezeshk *et al.*, 2011).

Conclusions

Ground-motion prediction equations have been developed for earthquakes in southeastern Australia using reinterpreted source and attenuation parameters for small-to-moderate magnitude local earthquakes and a dataset augmented with recent significant earthquakes. A new Australian-specific coda duration model has also been developed, which is an important component of the random vibration process in the stochastic ground-motion theory. The GMPEs are applicable for earthquakes from $4.0 \leq M_W \leq 7.5$ and R_{rup} distances less than 400 km. The GMPEs are compared to moderate-magnitude earthquake data recorded from southeastern Australian earthquakes. The models indicate low residuals across the full magnitude and distance range considered.

Through the empirical analysis of earthquake source parameters for southeastern Australian earthquakes, it was observed that high-quality Brune stress drops tend to vary with hypocentral depth. Average Brune stress drop for shallow earthquakes (h < 10 km) is approximately 23 MPa, while deeper earthquakes ($h \geq 10$ km) have an average stress drop of 50 MPa. While these stress drops may appear larger than those generally considered appropriate for intraplate regions, they are consistent with recent values determined in ENA (e.g., Boore, 2012), and the values are internally consistent with the path attenuation parameters derived in the present study. A significant distinction between the GMPE herein, and other published GMPEs for stable continental regions, is that the GMPE allows for a depth-dependent stress drop. The primary benefit is that the two models allow for different spectral shapes for shallow and deep earthquakes, particularly at high frequencies (Figs. 17-19). Differences in spectral shapes for shallow and deep earthquakes are observed empirically (Fig.11).

Finally, a correlation between measured V_{S30} and κ_0 was developed from the limited data available. While the correlation would be considered poorly constrained, a p-test indicated that the correlation is statistically significant. Assuming the correlation holds, a V_{S30} of approximately 820 m/s is obtained at a κ_0 of 0.006 sec based on the regression procedure used herein. Consequently, the GMPE presented herein can be considered appropriate for Australian B/C boundary rock sites under the modified NEHRP (Wills et al., 2000) site classification scheme.

The analysis and models presented here represent a significant advance in Australian ground-motion attenuation modelling. While the models could be enhanced further, in their present form they are consistent with the requirements of the Australian Standards and should not require any further adjustments for use in the revision of the Australian earthquake hazard map (Burbidge and Leonard, 2011; Burbidge, 2012). Furthermore, the models presented herein can also be used to provide more realistic hazard inputs to Australian earthquake risk assessments, as well as for use in rapid decision support tools for future earthquake events (e.g., Wald *et al.*, 1999; Earle *et al.*, 2009)

Data and Resources

Figure 2 was generated using Generic Mapping Tools (Wessel and Smith, 1991). The backdrop uses the General Bathymetric Chart of the Oceans bathymetry and topography dataset (http://www.gebco.net/data_and_products/gridded_bathymetry_data/). All Matlab modules used in the derivation of attenuation and source parameters, as well as some sample ground-motion data as used by the author, can be made available upon request.

Acknowledgments

References

Abercrombie, R. E. (1995). Earthquake source scaling relationships from -1 to 5 M_L using seismograms recorded at 2.5-km depth, *J. Geophys. Res.* **100,** 24,015-24,036.

Abercrombie, R. E., and P. Leary (1993). Source parameters of small earthquakes recorded at 2.5 km depth, Cajon Pass, southern California: implications for earthquake scaling, *Geophys. Res. Lett.* **20,** 1511-1514.

Abrahamson, N., G. Atkinson, D. Boore, Y. Bozorgnia, K. Campbell, B. Chiou, I. M. Idriss, W. Silva, and R. Youngs (2008). Comparisons of the NGA ground-motion relations, *Earthq. Spectra* **24,** 45–66.

Allen, T., M. Leonard, and C. Collins (2011). The 2012 Australian Seismic Hazard Map – catalogue and ground motion prediction equations, *Proceedings of the 2011 Australian Earthquake Engineering Society Conference*, Barossa Valley, South Australia, Australian Earthquake Engineering Society.

Allen, T. I. (2010). The influence of attenuation in earthquake ground-motion and magnitude estimation: implications for Australian earthquake hazard, *Proc. 2010 Aust. Earthq. Eng. Soc. Conf.*, Perth, Western Australia.

Allen, T. I., and G. M. Atkinson (2007). Comparison of earthquake source spectra and attenuation in eastern North America and southeastern Australia, *Bull. Seism. Soc. Am.* **97,** 1350–1354.

Allen, T. I., P. R. Cummins, T. Dhu, and J. F. Schneider (2007). Attenuation of ground-motion spectral amplitudes in southeastern Australia, *Bull. Seism. Soc. Am.* **97,** 1279–1292.

Allen, T. I., T. Dhu, P. R. Cummins, and J. F. Schneider (2006). Empirical attenuation of ground-motion spectral amplitudes in southwestern Western Australia, *Bull. Seism. Soc. Am.* **96,** 572-585.

Allen, T. I., G. Gibson, A. Brown, and J. P. Cull (2004). Depth variation of seismic source scaling relations: implications for earthquake hazard in southeastern Australia, *Tectonophys.* **390,** 5-24.

Allmann, B. P., and P. M. Shearer (2007). Spatial and temporal stress drop variations in small earthquakes near Parkfield, California, *J. Geophys. Res.* **112,** B04305.

Allmann, B. P., and P. M. Shearer (2009). Global variations of stress drop for moderate to large earthquakes, *J. Geophys. Res.* **114,** B01310.

Ambraseys, N. N., J. Douglas, S. K. Sarma, and P. M. Smit (2005). Equations for the estimation of strong ground motions from shallow crustal earthquakes using data from Europe and the Middle East: horizontal peak ground acceleration and spectral acceleration, *Bull. Earthq. Eng.* **3,** 1–53.

Anderson, J. G., and S. E. Hough (1984). A model for the shape of the Fourier amplitude spectrum of acceleration at high frequencies, *Bull. Seism. Soc. Am.* **74,** 1969-1993.

Atkinson, G. M. (1993). Earthquake source spectra in eastern North America, *Bull. Seism. Soc. Am.* **83,** 1778-1798.

Atkinson, G. M. (1993). Notes on ground motion parameters for eastern North America: duration and H/V ratio, *Bull. Seism. Soc. Am.* **83,** 587-596.

Atkinson, G. M. (1996). The high-frequency shape of the source spectrum for earthquakes in eastern and western Canada, *Bull. Seism. Soc. Am.* **86,** 106-112.

Atkinson, G. M. (2004). Empirical attenuation of ground-motion spectral amplitudes in southeastern Canada and the northeastern United States, *Bull. Seism. Soc. Am.* **94,** 1079-1095.

Atkinson, G. M., K. Assatourians, D. M. Boore, K. Campbell, and D. Motazedian (2009). A guide to differences between stochastic point-source and stochastic finite-fault simulations, *Bull. Seism. Soc. Am.* **99,** 3192–3201.

Atkinson, G. M., and D. M. Boore (1995). Ground-motion relations for eastern North America, *Bull. Seism. Soc. Am.* **85,** 17-30.

Atkinson, G. M., and D. M. Boore (2006). Earthquake ground-motion predictions for eastern North America, *Bull. Seism. Soc. Am.* **96,** 2181-2205.

Atkinson, G. M., and D. M. Boore (2011). Modifications to existing ground-motion prediction equations in light of new data, *Bull. Seism. Soc. Am.* **101,** 1121–1135.

Atkinson, G. M., and R. F. Mereu (1992). The shape of ground motion attenuation curves in southeastern Canada, *Bull. Seism. Soc. Am.* **82,** 2014-2031.

Atkinson, G. M., and M. Morrison (2009). Observations on regional variability in ground-motion amplitudes for small-to-moderate earthquakes in North America, *Bull. Seism. Soc. Am.* **99,** 2393–2409.

Bay, F., D. Fäh, L. Malagnini, and D. Giardini (2003). Spectral shear-wave ground-motion scaling in Switzerland, *Bull. Seism. Soc. Am.* **93,** 414–429.

Bommer, J. J., F. Scherbaum, H. Bungum, F. Cotton, F. Sabetta, and N. A. Abrahamson (2005). On the use of logic trees for ground-motion prediction equations in seismic-hazard analysis, *Bull. Seism. Soc. Am.* **95,** 377–389.

Boore, D. M. (1983). Stochastic simulation of high-frequency ground motions based on seismological models of the radiated spectra, *Bull. Seism. Soc. Am.* **73,** 1865-1894.

Boore, D. M. (2003). Simulation of ground motion using the stochastic method, *Pure appl. geophys.* **160,** 635-676.

Boore, D. M. (2009). Comparing stochastic point-source and finite-source ground-motion simulations: SMSIM and EXSIM, *Bull. Seism. Soc. Am.* **99,** 3202–3216.

Boore, D. M. (2012). Updated determination of stress parameters for nine well-recorded earthquakes in eastern North America, *Seism. Res. Lett.* **83,** 190-199.

Boore, D. M., and J. Boatwright (1984). Average body-wave radiation coefficients, *Bull. Seism. Soc. Am.* **74,** 1615-1621.

Boore, D. M., K. W. Campbell, and G. M. Atkinson (2010). Determination of stress parameters for eight well-recorded earthquakes in eastern North America, *Bull. Seism. Soc. Am.* **100,** 1632–1645.

Boore, D. M., W. B. Joyner, and L. Wennerberg (1992). Fitting the stocastic ω^{-2} source model to observed response spectra in western North America: trade-offs between $\Delta\sigma$ and κ, *Bull. Seism. Soc. Am.* **82,** 1956-1963.

Bowman, J. R., and Kennett, B. L. N. (1991). Propagation of *Lg* waves in the north Australian craton: influence of crustal velocity gradients, Bull. Seism. Soc. Am. 81, 592-610.

Brune, J. N. (1970). Tectonic stress and the spectra of seismic shear waves from earthquakes, *J. Geophys. Res.* **75,** 4997-5009.

Brune, J. N. (1971). Correction, *J. Geophys. Res.* **76,** 5002.

Building Seismic Safety Council (2003). NEHRP Recommended Provisions for seismic regulations for new buildings and other structures, 2003 edition. Washington, D.C., Federal Emergency Management Agency **450,** 338 pp.

Bungum, H., S. Vaage, and E. S. Husebye (1982). The Meløy earthquake sequence, northern Norway: source parameters and their scaling relations, *Bull. Seism. Soc. Am.* **72,** 197-206.

Burbidge, D., and M. Leonard (2011). The 2012 Australian Seismic Hazard Map – draft maps, *Proceedings of the 2011 Australian Earthquake Engineering Society Conference*, Barossa Valley, South Australia, Australian Earthquake Engineering Society.

Burbidge, D. R., Ed. (2012). *The 2012 Australian Earthquake Hazard Map*, Geoscience Australia, Record 2012/XX.

Burbidge, D. R., T. Allen, C. Collins, A. McPherson, B. Drummond, M. Leonard, D. Clark, P. Cummins, R. Cuthbertson, M. Dentith, B. Gaull, G. Gibson, M. Leiba, D. Love, K. McCue, P. Somerville, J. Rynn, and J. Wilson (2010). Future directions for the National Earthquake Hazard Map for Australia, *Geoscience Australia Record 2010/04*. Canberra, Geoscience Australia 26 pp.

Burger, R. W., P. G. Somerville, J. S. Barker, R. B. Herrmann, and D. V. Helmberger (1987). The effect of crustal structure on strong ground motion attenuation relations in eastern North America, *Bull. Seism. Soc. Am.* **77,** 420-439.

Campbell, K. W. (2003). Prediction of strong ground motion using the hybrid empirical method and its use in the development of ground-motion (attenuation) relations in eastern North America, *Bull. Seism. Soc. Am.* **93,** 1012–1033.

Campbell, K. W. (2009). Estimates of shear-wave Q and κ_0 for unconsolidated and semiconsolidated sediments in eastern North America, *Bull. Seism. Soc. Am.* **99,** 2365–2392.

Campbell, K. W. (2011). Ground motion simulation using the hybrid empirical method: issues and insights, *Geot Geol Earthquake* **14,** 81-95.

Castellaro, S., F. Mulargia, and P. L. Rossi (2008). Vs30: proxy for seismic amplification?, *Seism. Res. Lett.* **79,** 540-543.

Chandler, A. M., N. T. K. Lam, and H. H. Tsang (2006). Near-surface attenuation modelling based on rock shear-wave velocity profile, *Soil Dyn. Earthq. Eng.* **26,** 1004-1014.

Chapman, M. C., and R. W. Godbee (2010). Investigation into the nature of vertical strong ground motion, Final Technical Report Award Number G09AP00074, Virginia Polytechnic Institute and State University, Blacksburg, Virginia.

Chapman, M. C., and R. W. Godbee (2012). Modeling geometrical spreading and the relative amplitudes of vertical and horizontal high-frequency ground motions in eastern North America, *Bull. Seism. Soc. Am.* **102,** 1957–1975.

Chen, S.-Z., and G. M. Atkinson (2002). Global comparisons of earthquake source spectra, *Bull. Seism. Soc. Am.* **92,** 885–895.

Chiou, B., R. Youngs, N. Abrahamson, and K. Addo (2010). Ground-motion attenuation model for small-to-moderate shallow crustal earthquakes in California and its implications on regionalization of ground-motion prediction models, *Earthq. Spectra* **26,** 907–926.

Chiou, B. S.-J., and R. R. Youngs (2008). An NGA model for the average horizontal component of peak ground motion and response spectra, *Earthq. Spectra* **24,** 173–215.

Choi, Y., and J. P. Stewart (2005). Nonlinear site amplification as function of 30 m shear wave velocity, *Earthquake Spectra* **21,** 1-30.

Civil Engineers Australia (2012). Victorian earthquakes increase damage assessment demand, *Civil Engineers Australia* **September 2012,** 68.

Collins, C., R. Kayen, B. Carkin, T. Allen, P. Cummins, and A. McPherson (2006). Shear wave velocity measurement at Australian ground motion seismometer sites by the spectral analysis of surface waves (SASW) method, *Earthquake Engineering in Australia, Proceedings: Australian Earthquake Engineering Society Conference, Canberra, ACT,*.

Collins, C. D. N., B. J. Drummond, and M. G. Nicoll (2003). Crustal thickness patterns in the Australian continent, *Evolution and dynamics of the Australian Plate*. R. R. Hillis, and R. D. Müller. Boulder, CO, Geological Society of America. **Geol. Soc. Australia Spec. Publ. 22, and Geol. Soc. America Spec. Pap. 372,** 121–128.

Dainty, A. M. (1981). A scattering model to explain seismic Q observations in the lithosphere between 1 and 30 Hz, *Geophys. Res. Lett.* **8,** 1126-1128.

Dhu, T., and T. Jones (2002). Earthquake risk in Newcastle and Lake Macquarie, *Geoscience Australia Record 2002/15*.

Douglas, J., P. Gehl, L. F. Bonilla, and C. Gélis (2010). A κ model for mainland France, *Pure Appl. Geophys.* **167,** 1303-1315.

Drouet, S., F. Cotton, and P. Guéguen (2010). v_{S30}, κ, regional attenuation and M_W from accelerograms: application to magnitude 3–5 French earthquakes, *Geophys. J. Int.* **182,** 880-898.

Earle, P. S., D. J. Wald, K. S. Jaiswal, T. I. Allen, M. G. Hearne, K. D. Marano, A. J. Hotovec, and J. M. Fee (2009). Prompt Assessment of Global Earthquakes for Response (PAGER): A system for rapidly determining the impact of earthquakes worldwide, U.S. Geological Survey Open-File Report 2009–1131. Golden 15 pp.

Edwards, B., D. Fäh, and D. Giardini (2011). Attenuation of seismic shear wave energy in Switzerland, *Geophys. J. Int.* **185,** 967–984.

Edwards, B., A. Rietbrock, J. J. Bommer, and B. Baptie (2008). The acquisition of source, path, and site effects from microearthquake recordings using Q tomography: application to the United Kingdom, *Bull. Seism. Soc. Am.* **98,** 1915–1935.

Electric Power Research Institute (2003). CEUS Ground Motion Project: Model Development and Results, Electric Power Research Institute Report 1008910. EPRI. Palo Alto, CA 105.

Gaull, B. A., M. O. Michael-Leiba, and J. M. W. Rynn (1990). Probabilistic earthquake risk maps of Australia, *Aust. J. Earth. Sci.* **37,** 169-187.

Geoscience Australia (2004). Newcastle Earthquake, Geoscience Australia, Canberra, http://www.ga.gov.au/image_cache/GA10000.pdf.

Goulet, C., N. Abrahamson, and Y. Bozorgnia (2011). NGA-East final project plan, Pacific Earthquake Engineering Research Center (PEER), Berkeley, CA 34 pp.

Haimson, B. C. (1978). Crustal stress in the Michigan Basin, *J. Geophys. Res.* **83,** 5857-5863.

Hanks, T. C., and H. Kanamori (1979). A moment magnitude scale, *J. Geophys. Res.* **84,** 2348-2350.

Hanks, T. C., and M. Wyss (1972). The use of body-wave spectra in the determination of seismic-source parameters, *Bull. Seism. Soc. Am.* **62,** 561-589.

Hartzell, S. H. (1978). Earthquake aftershocks as Green's Functions, *Geophys. Res. Lett.* **5,** 1-4.

Hashash, Y., K. Campbell, E. Rathje, W. Silva, J. Stewart, and A. Kottke (2011). Selected reference rock and issues for the CEUS, *Next Generation Attenuation for CEUS (NGA-East) Workshop 2*, Berkeley, CA.

Herrmann, R. B., and A. Kijko (1983). Modeling some empirical vertical component *Lg* relations, *Bull. Seism. Soc. Am.* **73,** 157-171.

Hough, S. E., J. G. Anderson, J. Brune, F. Vernon, G. Berger, J. Fletcher, L. Haar, T. Hanks, and L. Baker (1988). Attenuation near Anza, California, *Bull. Seism. Soc. Am.* **78,** 672-691.

Insurance Council of Australia. (2012). Insurance Council of Australia - historical disaster statistics, Retrieved 30 March 2012, from http://www.insurancecouncil.com.au/Default.aspx?tabid=1572.

Kayen, R., and B. Carkin (2006). Preliminary report on the shear wave velocity of Australian strong motion seismometer sites by the Spectral Analysis of Surface Waves method (SASW) with parallel-arrayed harmonic-wave sources and H/V microtremor method, *U.S. Geological Survey Administritive Report 2006-2*, Menlo Park, CA 30 pp.

Kayen, R., B. Carkin, and D. Minasian (2010). Shear wave velocity of Australian strong motion seismometer sites by the Spectral Analysis of Surface Waves method (SASW): 2010 Survey, U.S. Geological Survey, Menlo Park, CA 33 pp.

Lam, N. T. K., and J. L. Wilson (2008). The new response spectrum model for Australia, **Special Issue: Earthquake Engineering in the Low and Moderate Seismic Regions of Southeast Asia and Australia,** 6-24.

Leonard, M. (2010). Earthquake fault scaling: self-consistent relating of rupture length, width, average displacement, and moment release, *Bull. Seism. Soc. Am.* **100,** 1971–1988.

Leonard, M., D. Robinson, T. Allen, J. Schneider, D. Clark, T. Dhu, and D. Burbidge (2007). Toward a better model of earthquake hazard in Australia, *Continental intraplate earthquakes: science, hazard, and policy issues.* S. Stein, and S. Mazzotti. Boulder, CO, The Geological Society of America. **Special Paper 425,** 263-283.

Liang, J. Z., H. Hao, B. A. Gaull, and C. Sinadinovski (2008). Estimation of strong ground motions in southwest Western Australia with a combined Green's function and stochastic approach, *J. Earthq. Eng.* **12,** 382–405.

McCue, K., V. Wesson, and G. Gibson (1990). The Newcastle, New South Wales, earthquake of 28 December 1989, *BMR J. Aust. Geol. Geophys.* **11,** 559–567.

Morozov, I. B. (2008). Geometrical attenuation, frequency dependence of *Q*, and the absorption band problem, *Geophys. J. Int.* **175,** 239–252.

Morozov, I. B. (2009). Thirty years of confusion around "scattering *Q*"?, *Seism. Res. Lett.* **80,** 5-7.

Motazedian, D., and G. M. Atkinson (2005). Stochastic finite-fault modeling based on a dynamic corner frequency, *Bull. Seism. Soc. Am.* **95,** 995–1010.

Nuttli, O. W. (1983). Average seismic source-parameter relations for mid-plate earthquakes, *Bull. Seism. Soc. Am.* **73,** 519-535.

Ou, G.-B., and R. B. Herrmann (1990). Astatistical model for ground motion produced by earthquakes at loacl and regional distances, *Bull. Seism. Soc. Am.* **80,** 1397-1417.

Petersen, M. D., A. D. Frankel, S. C. Harmsen, C. S. Mueller, K. M. Haller, R. L. Wheeler, R. L. Wesson, Y. Zeng, O. S. Boyd, D. M. Perkins, N. Luco, E. H. Field, C. J. Wills, and K. S. Rukstales (2008). Documentation for the 2008 update of the United States National Seismic Hazard Maps, *U.S. Geological Survey Open-File Report 2008–1128* 128 pp.

Pezeshk, S., A. Zandieh, and B. Tavakoli (2011). Hybrid empirical ground-motion prediction equations for eastern North America using NGA models and updated seismological parameters, *Bull. Seism. Soc. Am.* **101,** 1859–1870.

Power, M., B. Chiou, N. Abrahamson, Y. Bozorgnia, T. Shantz, and C. Roblee (2008). An overview of the NGA project, *Earthq. Spectra* **24,** 3–21.

Raoof, M., R. B. Herrmann, and L. Malagnini (1999). Attenuation and excitation of three-component ground motion in southern California, *Bull. Seism. Soc. Am.* **89,** 888-902.

Scholz, C. H., C. A. Aviles, and S. G. Wesnousky (1986). Scaling differences between large interplate and intraplate earthquakes, *Bull. Seism. Soc. Am.* **76,** 65-70.

Schorlemmer, D., S. Wiemer, and M. Wyss (2005). Variations in earthquake-size distribution across different stress regimes, *Nature* **437,** 539-542.

Shi, J., W.-Y. Kim, and P. G. Richards (1998). The corner frequencies and stress drops of intraplate earthquakes in the northeastern United States, *Bull. Seism. Soc. Am.* **88,** 531-542.

Somerville, P., N. Collins, R. Graves, S.-G. Song, and S. Ni (2009). Ground motion models for Australian earthquakes, Final Report. URS Corporation, Pasadena, CA.

Somerville, P., R. Graves, N. Collins, S.-G. Song, S. Ni, and P. Cummins (2009). Source and ground motion models for Australian earthquakes, The Australian Earthquake Engineering Society Conference. Newcastle.

Somerville, P. G., N. Collins, N. Abrahamson, G. R., and C. Saikia (2001). Earthquake source scaling and ground motion attenuation relations for the central and eastern United States, Final Report to the U.S. Geological Survey, Contract No. 99HQGR0098.

Standards Australia (2007). Structural design actions, part 4: Earthquake actions in Australia, Standards Australia 52.

The Mathworks (2008). Matlab: the language of technical computing, The Mathworks, Inc., Natick, MA.

Urbancic, T. I., C.-I. Trifu, J. M. Long, and R. P. Young (1992). Space-time correlations of *b* values with stress release, *Pure appl. geophys.* **139,** 450-462.

Van Houtte, C., S. Drouet, and F. Cotton (2011). Analysis of the origins of κ (kappa) to compute hard rock to rock adjustment factors for GMPEs, *Bull. Seism. Soc. Am.* **101,** 2926–2941.

Wald, D. J., V. Quitoriano, T. H. Heaton, H. Kanamori, C. W. Scrivner, and B. C. Worden (1999). TriNet "ShakeMaps": Rapid generation of peak ground-motion and intensity maps for earthquakes in southern California, *Earthq. Spectra* **15,** 537-556.

Wells, D. L., and K. J. Coppersmith (1994). New empirical relationships among magnitude, rupture length, rupture width, rupture area, and surface displacement, *Bull. Seism. Soc. Am.* **84,** 974 1002.

Wessel, P., and W. H. F. Smith (1991). Free software helps map and display data, *Eos Trans.* **72,** 441.

Wesson, V. (1988). Seismic modelling of the Victorian lithosphere, Phillip Institute of Technology, Melbourne. **MAppSc Thesis**.

Wilkie, J., and G. Gibson (1995). Estimation of seismic quality factor *Q* for Victoria, Australia, *AGSO J. Aust Geol. Geophys.* **15,** 511-517.

Wills, C. J., M. Petersen, W. A. Bryant, M. Reichle, G. J. Saucedo, S. Tan, G. Taylor, and J. Treiman (2000). A site-conditions map for California based on geology and shear-wave velocity, *Bull. Seism. Soc. Am.* **90,** S187–S208.

Appendix I

UNIT TEST DATA FOR ALLEN (2012) GMPE FOR EASTERN AUSTRALIA
DATA ARE INDICATED IN 5% DAMPED PSEUDO RESPONSE SPECTRAL ACCELERATION AT
DIFFERENT SPECTRAL PERIODS
FORMAT: PERIOD (SEC) LOG10 PSA (CM/S/S)

M_W = 4.5; R_{rup} = 20; h = 7
```
0.0100     1.2021
0.0200     1.3351
0.0300     1.4107
0.0500     1.4663
0.0750     1.4849
0.1000     1.4796
0.1500     1.4363
0.2000     1.3712
0.2500     1.3004
0.3000     1.2253
0.4000     1.0533
0.5000     0.8847
0.7500     0.5156
1.0000     0.2298
1.5000    -0.1924
2.0000    -0.4887
3.0000    -0.8921
4.0000    -1.1672
```
M_W = 4.5; R_{rup} = 20; h = 14
```
0.0100     1.2642
0.0200     1.4099
0.0300     1.5013
0.0500     1.5754
0.0750     1.5851
0.1000     1.5631
0.1500     1.4912
0.2000     1.3976
0.2500     1.2981
0.3000     1.1984
0.4000     0.9912
0.5000     0.8003
0.7500     0.3989
1.0000     0.0951
1.5000    -0.3380
2.0000    -0.6326
3.0000    -1.0265
4.0000    -1.2938
```

M_W = 4.5; R_{rup} = 50; h = 7
```
0.0100      0.5040
0.0200      0.6449
0.0300      0.7043
0.0500      0.7657
0.0750      0.7967
0.1000      0.8042
0.1500      0.7879
0.2000      0.7428
0.2500      0.6854
0.3000      0.6199
0.4000      0.4598
0.5000      0.2983
0.7500     -0.0624
1.0000     -0.3455
1.5000     -0.7717
2.0000     -1.0747
3.0000     -1.4856
4.0000     -1.7663
```
M_W = 4.5; R_{rup} = 50; h = 14
```
0.0100      0.5336
0.0200      0.6725
0.0300      0.7552
0.0500      0.8400
0.0750      0.8677
0.1000      0.8615
0.1500      0.8149
0.2000      0.7393
0.2500      0.6531
0.3000      0.5630
0.4000      0.3676
0.5000      0.1831
0.7500     -0.2099
1.0000     -0.5093
1.5000     -0.9482
2.0000     -1.2538
3.0000     -1.6602
4.0000     -1.9346
```
M_W = 4.5; R_{rup} = 100; h = 7
```
0.0100      0.0639
0.0200      0.1937
0.0300      0.2405
0.0500      0.3083
0.0750      0.3543
0.1000      0.3758
0.1500      0.3841
0.2000      0.3586
0.2500      0.3172
0.3000      0.2635
0.4000      0.1155
0.5000     -0.0422
0.7500     -0.3987
1.0000     -0.6777
1.5000     -1.1051
2.0000     -1.4137
3.0000     -1.8295
4.0000     -2.1118
```

M_W = 4.5; R_{rup} = 100; h = 14
```
0.0100      0.0742
0.0200      0.1952
0.0300      0.2711
0.0500      0.3618
0.0750      0.4071
0.1000      0.4171
0.1500      0.3932
0.2000      0.3354
0.2500      0.2648
0.3000      0.1869
0.4000      0.0041
0.5000     -0.1765
0.7500     -0.5653
1.0000     -0.8610
1.5000     -1.3017
2.0000     -1.6136
3.0000     -2.0282
4.0000     -2.3072
```
M_W = 4.5; R_{rup} = 200; h = 7
```
0.0100     -0.3488
0.0200     -0.2961
0.0300     -0.2658
0.0500     -0.2106
0.0750     -0.1453
0.1000     -0.0929
0.1500     -0.0224
0.2000      0.0124
0.2500      0.0273
0.3000      0.0184
0.4000     -0.0798
0.5000     -0.2179
0.7500     -0.5657
1.0000     -0.8479
1.5000     -1.2760
2.0000     -1.5813
3.0000     -1.9988
4.0000     -2.2852
```
M_W = 4.5; R_{rup} = 200; h = 14
```
0.0100     -0.3595
0.0200     -0.3094
0.0300     -0.2571
0.0500     -0.1841
0.0750     -0.1128
0.1000     -0.0641
0.1500     -0.0162
0.2000     -0.0091
0.2500     -0.0208
0.3000     -0.0527
0.4000     -0.1872
0.5000     -0.3521
0.7500     -0.7357
1.0000     -1.0321
1.5000     -1.4721
2.0000     -1.7820
3.0000     -2.1942
4.0000     -2.4735
```

M_W = 5.5; R_{rup} = 20; h = 7
```
0.0100      1.7698
0.0200      1.8800
0.0300      1.9405
0.0500      1.9940
0.0750      2.0206
0.1000      2.0286
0.1500      2.0193
0.2000      1.9911
0.2500      1.9557
0.3000      1.9134
0.4000      1.8019
0.5000      1.6847
0.7500      1.4121
1.0000      1.1907
1.5000      0.8310
2.0000      0.5577
3.0000      0.1659
4.0000     -0.1138
```
M_W = 5.5; R_{rup} = 20; h = 14
```
0.0100      1.9109
0.0200      2.0355
0.0300      2.0978
0.0500      2.1632
0.0750      2.1899
0.1000      2.1937
0.1500      2.1784
0.2000      2.1423
0.2500      2.0972
0.3000      2.0451
0.4000      1.9148
0.5000      1.7816
0.7500      1.4745
1.0000      1.2256
1.5000      0.8322
2.0000      0.5414
3.0000      0.1363
4.0000     -0.1452
```
M_W = 5.5; R_{rup} = 50; h = 7
```
0.0100      1.1383
0.0200      1.2479
0.0300      1.2957
0.0500      1.3542
0.0750      1.3939
0.1000      1.4142
0.1500      1.4270
0.2000      1.4166
0.2500      1.3957
0.3000      1.3645
0.4000      1.2666
0.5000      1.1564
0.7500      0.8924
1.0000      0.6752
1.5000      0.3178
2.0000      0.0436
3.0000     -0.3517
4.0000     -0.6354
```

$M_W = 5.5$; $R_{rup} = 50$; h = 14
0.0100	1.2533
0.0200	1.3665
0.0300	1.4292
0.0500	1.4984
0.0750	1.5407
0.1000	1.5600
0.1500	1.5666
0.2000	1.5472
0.2500	1.5163
0.3000	1.4754
0.4000	1.3589
0.5000	1.2325
0.7500	0.9334
1.0000	0.6888
1.5000	0.2960
2.0000	0.0025
3.0000	−0.4060
4.0000	−0.6902

$M_W = 5.5$; $R_{rup} = 100$; h = 7
0.0100	0.7692
0.0200	0.8587
0.0300	0.8963
0.0500	0.9603
0.0750	1.0144
0.1000	1.0484
0.1500	1.0836
0.2000	1.0928
0.2500	1.0896
0.3000	1.0719
0.4000	0.9858
0.5000	0.8765
0.7500	0.6145
1.0000	0.4047
1.5000	0.0486
2.0000	−0.2312
3.0000	−0.6282
4.0000	−0.9094

$M_W = 5.5$; $R_{rup} = 100$; h = 14
0.0100	0.8714
0.0200	0.9630
0.0300	1.0205
0.0500	1.0887
0.0750	1.1451
0.1000	1.1795
0.1500	1.2065
0.2000	1.2048
0.2500	1.1915
0.3000	1.1650
0.4000	1.0634
0.5000	0.9414
0.7500	0.6447
1.0000	0.4017
1.5000	0.0099
2.0000	−0.2851
3.0000	−0.7011
4.0000	−0.9904

M_W = 5.5; R_{rup} = 200; h = 7
```
0.0100      0.3700
0.0200      0.3983
0.0300      0.4183
0.0500      0.4671
0.0750      0.5343
0.1000      0.5932
0.1500      0.6815
0.2000      0.7440
0.2500      0.7911
0.3000      0.8139
0.4000      0.7735
0.5000      0.6830
0.7500      0.4288
1.0000      0.2142
1.5000     -0.1422
2.0000     -0.4165
3.0000     -0.8117
4.0000     -1.0953
```
M_W = 5.5; R_{rup} = 200; h = 14
```
0.0100      0.4681
0.0200      0.4978
0.0300      0.5325
0.0500      0.5869
0.0750      0.6551
0.1000      0.7146
0.1500      0.8047
0.2000      0.8617
0.2500      0.8989
0.3000      0.9115
0.4000      0.8523
0.5000      0.7455
0.7500      0.4563
1.0000      0.2141
1.5000     -0.1761
2.0000     -0.4690
3.0000     -0.8820
4.0000     -1.1711
```
M_W = 6.5; R_{rup} = 20; h = 7
```
0.0100      2.1974
0.0200      2.2994
0.0300      2.3485
0.0500      2.3940
0.0750      2.4187
0.1000      2.4302
0.1500      2.4370
0.2000      2.4265
0.2500      2.4071
0.3000      2.3803
0.4000      2.3019
0.5000      2.2162
0.7500      2.0138
1.0000      1.8482
1.5000      1.5694
2.0000      1.3511
3.0000      1.0329
4.0000      0.7969
```

$M_W = 6.5; \ R_{rup} = 20; \ h = 14$

0.0100	2.3755
0.0200	2.4887
0.0300	2.5246
0.0500	2.5820
0.0750	2.6141
0.1000	2.6278
0.1500	2.6377
0.2000	2.6281
0.2500	2.6079
0.3000	2.5789
0.4000	2.4935
0.5000	2.4001
0.7500	2.1763
1.0000	1.9905
1.5000	1.6784
2.0000	1.4361
3.0000	1.0873
4.0000	0.8336

$M_W = 6.5; \ R_{rup} = 50; \ h = 7$

0.0100	1.6338
0.0200	1.7267
0.0300	1.7669
0.0500	1.8168
0.0750	1.8549
0.1000	1.8783
0.1500	1.9020
0.2000	1.9070
0.2500	1.9030
0.3000	1.8888
0.4000	1.8255
0.5000	1.7467
0.7500	1.5529
1.0000	1.3931
1.5000	1.1226
2.0000	0.9093
3.0000	0.5915
4.0000	0.3531

$M_W = 6.5; \ R_{rup} = 50; \ h = 14$

0.0100	1.7919
0.0200	1.8891
0.0300	1.9343
0.0500	1.9894
0.0750	2.0347
0.1000	2.0637
0.1500	2.0923
0.2000	2.0980
0.2500	2.0927
0.3000	2.0763
0.4000	2.0063
0.5000	1.9202
0.7500	1.7044
1.0000	1.5228
1.5000	1.2176
2.0000	0.9805
3.0000	0.6373
4.0000	0.3852

M_W = 6.5; R_{rup} = 100; h = 7
```
0.0100      1.3271
0.0200      1.3951
0.0300      1.4271
0.0500      1.4801
0.0750      1.5306
0.1000      1.5666
0.1500      1.6113
0.2000      1.6354
0.2500      1.6494
0.3000      1.6491
0.4000      1.5978
0.5000      1.5192
0.7500      1.3264
1.0000      1.1745
1.5000      0.9054
2.0000      0.6870
3.0000      0.3705
4.0000      0.1372
```
M_W = 6.5; R_{rup} = 100; h = 14
```
0.0100      1.4803
0.0200      1.5549
0.0300      1.5937
0.0500      1.6425
0.0750      1.6975
0.1000      1.7396
0.1500      1.7881
0.2000      1.8118
0.2500      1.8250
0.3000      1.8240
0.4000      1.7705
0.5000      1.6898
0.7500      1.4750
1.0000      1.2924
1.5000      0.9887
2.0000      0.7536
3.0000      0.4038
4.0000      0.1469
```
M_W = 6.5; R_{rup} = 200; h = 7
```
0.0100      0.9423
0.0200      0.9655
0.0300      0.9788
0.0500      1.0147
0.0750      1.0713
0.1000      1.1253
0.1500      1.2130
0.2000      1.2832
0.2500      1.3414
0.3000      1.3771
0.4000      1.3679
0.5000      1.3080
0.7500      1.1228
1.0000      0.9650
1.5000      0.6955
2.0000      0.4844
3.0000      0.1728
4.0000      -0.0609
```

M_W = 6.5; R_{rup} = 200; h = 14
0.0100	1.1085
0.0200	1.1311
0.0300	1.1489
0.0500	1.1873
0.0750	1.2401
0.1000	1.2934
0.1500	1.3940
0.2000	1.4699
0.2500	1.5255
0.3000	1.5570
0.4000	1.5404
0.5000	1.4744
0.7500	1.2696
1.0000	1.0896
1.5000	0.7885
2.0000	0.5551
3.0000	0.2090
4.0000	−0.0464

M_W = 7.5; R_{rup} = 20; h = 7
0.0100	2.4859
0.0200	2.5942
0.0300	2.6357
0.0500	2.6674
0.0750	2.6802
0.1000	2.6855
0.1500	2.6901
0.2000	2.6780
0.2500	2.6554
0.3000	2.6267
0.4000	2.5538
0.5000	2.4796
0.7500	2.3213
1.0000	2.2029
1.5000	2.0232
2.0000	1.8923
3.0000	1.7097
4.0000	1.5655

M_W = 7.5; R_{rup} = 20; h = 14
0.0100	2.6588
0.0200	2.7703
0.0300	2.7825
0.0500	2.8330
0.0750	2.8589
0.1000	2.8669
0.1500	2.8706
0.2000	2.8563
0.2500	2.8315
0.3000	2.8011
0.4000	2.7285
0.5000	2.6570
0.7500	2.5058
1.0000	2.3914
1.5000	2.2024
2.0000	2.0532
3.0000	1.8284
4.0000	1.6445

M_W = 7.5; R_{rup} = 50; h = 7
```
0.0100      1.9904
0.0200      2.0813
0.0300      2.1180
0.0500      2.1535
0.0750      2.1799
0.1000      2.1965
0.1500      2.2130
0.2000      2.2141
0.2500      2.2075
0.3000      2.1929
0.4000      2.1364
0.5000      2.0691
0.7500      1.9193
1.0000      1.8081
1.5000      1.6428
2.0000      1.5225
3.0000      1.3442
4.0000      1.1992
```
M_W = 7.5; R_{rup} = 50; h = 14
```
0.0100      2.1494
0.0200      2.2405
0.0300      2.2708
0.0500      2.3132
0.0750      2.3500
0.1000      2.3728
0.1500      2.3923
0.2000      2.3919
0.2500      2.3826
0.3000      2.3660
0.4000      2.3102
0.5000      2.2466
0.7500      2.1032
1.0000      1.9931
1.5000      1.8169
2.0000      1.6806
3.0000      1.4699
4.0000      1.2917
```
M_W = 7.5; R_{rup} = 100; h = 7
```
0.0100      1.7366
0.0200      1.8028
0.0300      1.8324
0.0500      1.8671
0.0750      1.9023
0.1000      1.9298
0.1500      1.9664
0.2000      1.9858
0.2500      1.9957
0.3000      1.9940
0.4000      1.9505
0.5000      1.8852
0.7500      1.7368
1.0000      1.6312
1.5000      1.4641
2.0000      1.3401
3.0000      1.1658
4.0000      1.0270
```

M_W = 7.5; R_{rup} = 100; h = 14
```
0.0100      1.9002
0.0200      1.9705
0.0300      1.9903
0.0500      2.0226
0.0750      2.0636
0.1000      2.0969
0.1500      2.1375
0.2000      2.1560
0.2500      2.1650
0.3000      2.1634
0.4000      2.1248
0.5000      2.0681
0.7500      1.9253
1.0000      1.8104
1.5000      1.6340
2.0000      1.5016
3.0000      1.2858
4.0000      1.1042
```
M_W = 7.5; R_{rup} = 200; h = 7
```
0.0100      1.3672
0.0200      1.4052
0.0300      1.4155
0.0500      1.4317
0.0750      1.4651
0.1000      1.5025
0.1500      1.5714
0.2000      1.6294
0.2500      1.6775
0.3000      1.7071
0.4000      1.7025
0.5000      1.6564
0.7500      1.5159
1.0000      1.4039
1.5000      1.2363
2.0000      1.1207
3.0000      0.9541
4.0000      0.8168
```
M_W = 7.5; R_{rup} = 200; h = 14
```
0.0100      1.5614
0.0200      1.5902
0.0300      1.5916
0.0500      1.6167
0.0750      1.6417
0.1000      1.6716
0.1500      1.7513
0.2000      1.8152
0.2500      1.8587
0.3000      1.8834
0.4000      1.8766
0.5000      1.8342
0.7500      1.7037
1.0000      1.5940
1.5000      1.4210
2.0000      1.2893
3.0000      1.0782
4.0000      0.9001
```